Multiple intermediate states precede pore block during N-type inactivation of a voltage-gated potassium channel

Alison Prince-Carter and Paul J. Pfaffinger

Department of Neuroscience, Baylor College of Medicine, Houston, TX 77030

N-type inactivation of voltage-gated potassium channels is an autoinhibitory process that occurs when the N terminus binds within the channel pore and blocks conduction. N-type inactivation and recovery occur with single-exponential kinetics, consistent with a single-step reaction where binding and block occur simultaneously. However, recent structure–function studies have suggested the presence of a preinactivated state whose formation and loss regulate inactivation and recovery kinetics. Our studies on N-type inactivation of the Shaker-type AKv1 channel support a multiple-step inactivation process involving a series of conformational changes in distinct regions of the N terminus that we have named the polar, flex, and latch regions. The highly charged polar region forms interactions with the surface of the channel leading up to the side window openings between the T1 domain and the channel transmembrane domains, before the rate-limiting step occurs. This binding culminates with a specific electrostatic interaction between R18 and EDE161-163 located at the entrance to the side windows. The latch region appears to work together with the flex region to block the pore after polar region binding occurs. Analysis of tail currents for a latch region mutant shows that both blocked and unblocked states exist after the rate-limiting transition is passed. Our results suggest that at least two intermediate states exist for N-type inactivation: a polar region–bound state that is formed before the rate-limiting step, and a pre-block state that is formed by the flex and latch regions during the rate-limiting step.

The Journal of General Physiology

INTRODUCTION

During a membrane depolarization, many types of ion channels inactivate, losing their ability to conduct currents (Hille, 2001; Kurata and Fedida, 2006). In neurons, channel inactivation provides an important short-term regulatory signal that may also have a "memory" component where a recent history of membrane depolarization is encoded as a higher probability of being inactivated (Giese et al., 2001; Gilboa et al., 2005). In N-type inactivation, the cytoplasmic N termini of certain voltage-gated potassium (Kv) channel α subunits or auxiliary subunits block ions from conducting through the open-channel pore (Aldrich, 2001).

N-type inactivation has been studied by pharmacological, electrophysiological, nuclear magnetic resonance (NMR), and x-ray structural methods (Hoshi et al., 1990; Zagotta et al., 1990; Demo and Yellen, 1991; Murrell-Lagnado and Aldrich, 1993b; Antz et al., 1997; Zhou et al., 2001; Wissmann et al., 2003; Baker et al., 2006; Decher et al., 2008; Molina et al., 2008). The mechanism underlying N-type inactivation is proposed to be direct pore block, produced by binding of the N terminus within the inner vestibule of the transmembrane pore (Zagotta et al., 1990; Demo and Yellen, 1991; Murrell-Lagnado and Aldrich, 1993b). Specific results supporting this model include accelerated recovery by permeant ion "clearing," channel reopening from the inactivated state before closing at negative potentials, and competition with internal quaternary ammonium blockers, which bind to a position just below the K^+ channel selectivity filter, within the inner vestibule (Choi et al., 1991; Demo and Yellen, 1991; Zhou et al., 2001). In addition, mutations to hydrophobic residues lining the internal vestibule energetically couple with residues at the N terminus of the inactivation domain (Zhou et al., 2001; Decher et al., 2008). Access of the N terminus to the pore block site depends on voltage-dependent activation gating, resulting in a gating cycle where the channel inactivates at positive potentials after the channel opens and recovers at negative potentials after the "ball" is released and the channel closes (Fig. 1 A).

N-type inactivation has been primarily described by two kinetic models: a single-step inactivation model and a two-step (preinactivation) model (Fig. 1, B and C) (Hoshi et al., 1990; Zhou et al., 2001). The original single-step inactivation model proposed that binding and blocking occur simultaneously (Fig. 1 B). The preinactivation model hypothesized that formation and loss of a distinct intermediate state, called the "preinactivated" state, is rate limiting for macroscopic inactivation and

Correspondence to Paul J. Pfaffinger: paulp@bcm.tmc.edu

Abbreviations used in this paper: Kv, voltage-gated potassium; NMR, nuclear magnetic resonance; VMD, visual molecular dynamics.

The Rockefeller University Press $30.00
J. Gen. Physiol. Vol. 134 No. 1 15–34
www.jgp.org/cgi/doi/10.1085/jgp.200910219

recovery kinetics. In this model, the actual pore block and unblock kinetics are not directly observable because these kinetics collapse into the rate-limiting preinactivation transitions, making the reaction pseudo first order and thus single exponential.

The pore-blocking region of the N terminus called the 'ball" is encoded within the first ~20 residues. The preinactivation model further divides the 20 residues of the ball into two distinct regions, a hydrophobic region, residues 1–7, that binds within the pore and blocks conductance, and the remaining hydrophilic region, which is involved in forming the preinactivated state. The remainder of the N terminus is thought to act as an unstructured tether, the "chain," whose length but not sequence regulates pore block kinetics (Hoshi et al., 1990). The pore-blocking activity of ball peptides changes depending on the hydrophobicity and charge of the substitutions that are made to the ball peptide. In general, peptides that are more hydrophobic and more positively charged are found to have the highest affinity, suggesting that a combination of electrostatic steering and hydrophobic interactions regulates N-type inactivation (Demo and Yellen, 1991; Murrell-Lagnado and Aldrich, 1993a,b). The electrostatic steering has been described as a "long-range" effect, rather than being due to specific interactions between the peptide and channel because a variety of substitutions within these peptides produce the same effects (Zagotta et al., 1990; Murrell-Lagnado and Aldrich, 1993a).

In this study, we have examined the extent and type of interactions occurring between the N terminus and the channel core of the Aplysia Shaker-type channel, AKv1. Our results indicate that N-type inactivation of the AKv1 channel is a multistep process that involves the formation of an intermediate state where much of the N terminus of the channel is bound to the cytoplasmic surface of the open channel. Formation of this intermediate state appears to be a critical step in N-type inactivation of the AKv1 channel, allowing the N terminus to access the transmembrane pore. After completion of the rate-limiting step to inactivate, our data suggest that at least two conformational states exist, a pre-block state and a pore block state. Although both states recover with similar kinetics, the conductance pathway is only disabled in the pore block state.

MATERIALS AND METHODS

Molecular methods

Experiments were performed on the Aplysia Shaker-type Kv channel (AKv1; M95914), which has a well-characterized, robust N-type inactivation (Pfaffinger et al., 1991; Furukawa and Takahashi, 1997). The AKv1 coding sequence was cloned into the pBS-II vector (Agilent Technologies). Mutations were introduced into the AKv1 cDNA by PCR (QuiKChange kit; Agilent Technologies) or by cassette cloning of double stranded. All mutant constructs were verified by DNA sequencing on both strands through the entire coding sequence. Message RNA was made using the mMESSAGE mMACHINE kit (Applied Biosystems).

Homology analysis was performed on several vertebrate and invertebrate Shaker channel N-terminal sequences with known N-type inactivation properties, including vertebrate Kv1.4 channels, tunicate Halocynthia TuKv1 channel (Lee et al., 1996; Ono et al., 1999), and the ShB and Kvβ1.1 sequences because they are the basis for the current models on N-type inactivation (Hoshi et al., 1990; Zhou et al., 2001). Sequences were aligned in a gap-free manner from the initiator Met, except that (1) ShB aligned best-shifted 1 residue to the right; (2) two insertions were needed in Fugu Kv1.4 to maintain its alignment with rat Kv1.4; and (3) residue S10 in the Halocynthia TnKv1 sequence was not aligned to maintain a conserved alignment with glycine residues in other sequences. A consensus sequence covering all 12 residues of the latch and flex regions was made based on the criteria that at least half of the residues at the aligned site are identical or have the same polarity (hydrophobic or polar). Percent similarity to the consensus was calculated by scoring 3 points for a sequence identity match, 2 points for a polarity identity match, and 1 point for consensus sequence mismatch if the mismatched residue has the same polarity, or in the case of glycine, the substituted residue is a small polar residue–like serine and dividing by the similarity score for the consensus sequence (34 points). Secondary structure analysis and β turn propensity was evaluated using the COUDES server, which combines secondary structure propensities with position-specific scoring matrices (Fuchs and Alix, 2005).

Electrophysiological recordings

K^+ currents (1–3 μA) were recorded from mRNA-injected *Xenopus* oocytes at 1–3 d after injection using a two-electrode voltage clamp (Warner Instruments) with currents filtered at 1 kHz (902; Frequency Devices). Electrodes were filled with 3 M KCl with tip resistances of 0.5–1 MΩ for the voltage electrode and 0.1–0.5 MΩ with an agar tip plug for the current electrode. Standard protocols for the recording of steady-state and kinetic properties for activation, inactivation, and recovery from inactivation for channel constructs were used (Pfaffinger et al., 1991; Cushman et al., 2000; Jerng et al., 2004, 2005, 2007; Baker et al., 2006). Time constants for inactivation and recovery are compared at +50 and −100 mV, respectively. Multiple recording sessions in different oocyte preps were performed for each mutant to control for potential oocyte variability. WinWCP (Strathclyde Electrophysiology Software) controlling a NIDAQ PCI-6019 B series A/D board (National Instruments Corp.) or pClamp6 and a Digidata 1200 A/D board (MDS Analytical Technologies) were used to conduct recordings and analyze data. Leak current subtraction was performed by using a P/4 protocol. Elevated extracellular K^+ was used to suppress C-type inactivation in the AKv1 channel while allowing us to study N-type inactivation (see Fig. S1) (Baukrowitz and Yellen, 1995; Furukawa and Takahashi, 1997). The normal Hi K^+ bath solution is (in mM): 98 KCl, 1 $MgCl_2$, 1.8 $CaCl_2$, and 5 HEPES, pH 7.4. DIDS (4,4'-diisothiocyano-2,2'-stilbene disulphonic acid) was added to block endogenous chloride currents. For low K^+ recordings, the bath solution was normal ND-96 (in mM: 96 NaCl, 2 KCl, 1.8 $CaCl_2$, 1 $MgCl_2$, and 5 HEPES, with pH adjusted with NaOH to 7.4).

Data analysis

Data analysis was performed and graphs were generated using a combination of WinWCP, Origin 6.1 (Origin Laboratories), and Excel (Microsoft). Measured time constants are reported as the mean ± SEM (n, number of independent measurements). Error propagations from measured time constants to energetic estimates were performed using standard propagation formulae

(Croarkin, 2008). Significance testing was performed using an independent *t* test with the significance level set at 0.05. Significance levels in the tables are indicated ($P < 0.05$ and $P < 0.01$). The time constants for inactivation and recovery were measured by either single-exponential fitting or by double-exponential fitting where the slower time constant was fixed to eliminate the effect of residual C-type inactivation (see Fig. S1). For constructs where >95% of the total current inactivated in the fast component, we assume that the inverse of the measured τ_{in} is a good estimate of the rate-limiting step to inactivate. For a few constructs, such as EVA(2–4)ATT, there is significant residual current at the end of the pulse. In this case, under a single-step model, the measured τ_{in} is reduced by the large reverse rate constant. We can adjust for this effect by calculating τ_{on}:

$$\tau_{on} = \frac{\tau_{in}}{f_I},$$

where f_I is the fraction of current that inactivated in the pulse. In multistep models, there is no general correction to relate a measured inactivation time constant to the rate-limiting kinetics rate constant; however, the inverses of τ_{on} and τ_{in} provide reasonable bounds for the underlying rate.

Energetic measurements and electrostatic tests

Energetic analyses were performed using a pseudo first-order model (appropriate because N-type inactivation has single-exponential inactivation and recovery kinetics), where ON and recovery reactions pass through a common rate-limiting transition (Fig. 1, B and C). In this case, the reaction is described as a conformational change involving the N terminus being either free or bound. Voltage steps to positive and negative potentials reveal the size of the energy jumps to the rate-limiting transition state for the on and recovery processes. As described previously, τ_{in} or τ_{on} was used to estimate the underlying on rate–limiting step to inactivate, and τ_{recov} was used to estimate the underlying recovery rate-limiting step. Free energy to the transition state for the rate-limiting ON and recovery processes was measured as:

$$\Delta G = kT \ln(\tau / \text{msec}),$$

using the appropriate time constant measured in milliseconds, which normalizes our energetics to the fastest relevant process we can measure in our system, 1 kHz. The apparent equilibrium constant for the free–bound reaction, K_{eq}, is taken as:

$$K_{eq} = \frac{\tau_{ON}}{\tau_{Recov}},$$

where τ_{ON} is either the inactivation time constant (τ_{in}) or the adjusted time constant (τ_{on}). Likewise, we estimate the equilibrium energy difference as: $\Delta G(K_{eq}) = \Delta G(\tau_{ON}) - \Delta G(\tau_{Recov})$.

The thermodynamic coupling coefficient between a core channel site and an N-terminal site was calculated for the ON or recovery processes as:

$$\Omega = \frac{\tau_{WT,WT} \times \tau_{MT,MT}}{\tau_{WT,MT} \times \tau_{MT,WT}},$$

using the appropriate time constant.

For electrostatic measurements, the free energy of the inactivation ON and recovery reactions was compared with the charge present at the N-terminal residue being probed (+1 R,K; 0 A; −1 D,E). In addition, double mutations combining charge changes in the channel core and the N terminus were used to determine the contribution of the core residue site to the electrostatic potential change felt by the N terminus during the inactivation reaction. A linear relationship between the change in free energy compared with the change in charge is indicative of an electrostatic energy relationship. Electrostatic potentials are reported in terms of the potential difference experienced by the N-terminal residue during the examined transition.

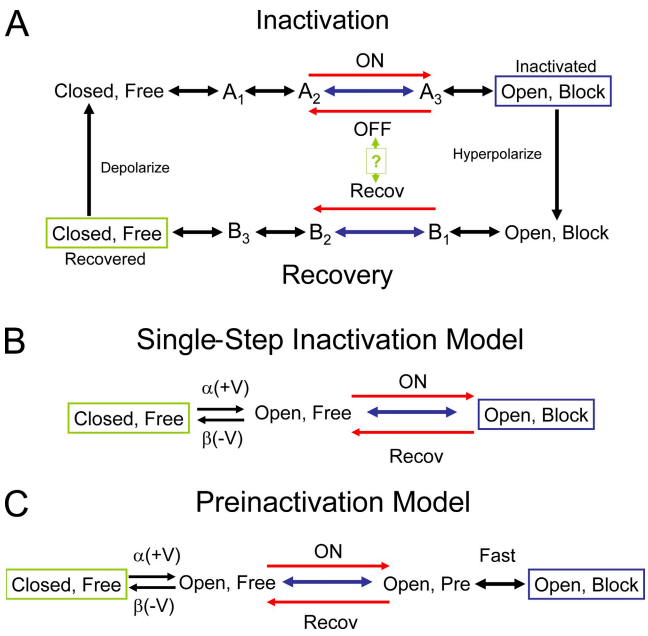

Figure 1. N-type inactivation gating models. Stable terminal states boxed: green, hyperpolarized; blue, depolarized. Rate-limiting transitions in blue with key rate-limiting directional reactions in red. (A) General gating cycle where depolarization gates the formation of the opened state from which the free N terminus can bind to the channel to block it. The number of steps between these two states is unknown, but at some point in the chain the rate-limiting transition occurs for the ON and OFF reactions. At hyperpolarized potentials, the channel gates from the open blocked state back to the closed free state. The rate-limiting step for recovery occurs somewhere along this chain and may or may not be identical to the rate-liming OFF step at depolarized potentials. (B) Single-step inactivation model. Model incorporates a single block ON and recovery transition after channel voltage–dependent gating. Voltage dependence for inactivation is due to the voltage-dependent formation of the open state. (C) Preinactivation model. Model is similar to the single-step inactivation model, except an intermediate preinactivated state is proposed to occur between open and inactivated. Model proposes that the formation and breakdown of this preinactivated state are rate limiting for both inactivation and recovery.

Structural modeling

Structural modeling was performed using visual molecular dynamics (VMD) and DeepView (Humphrey et al., 1996; Guex and Peitsch, 1997). The Kv channel structure (accession no. 2R9R in the RCSB Protein Data Bank) was used as a template to construct an AKv1 transmembrane structural model (Long et al., 2007). The determined structure for the AKv1 T1 domain was RMSD aligned with the Kv1.2 T1 domain using VMD and then grafted onto our AKv1 transmembrane model. The channel tetramer was formed using the 2R9R transforms. After energy minimization using NAMD, a fully hydrated and ionized molecular dynamics system with the AKv1 model integrated into a DOPC membrane was then built using VMD (Humphrey et al., 1996;

Phillips et al., 2005). Extended molecular dynamics simulations were run using NAMD on the TACC Lonestar supercomputer through TeraGrid to minimize and equilibrate the model (Phillips et al., 2005). An inactivation domain model for AKv1 was constructed de novo based on the Kv1.4 N terminus structural model (Wissmann et al., 2003). The constructed AKv1 models were then prepared for electrostatics calculations using VMD and submitted to the APBS server. Models and electrostatic potentials were visualized using VMD and POV-Ray.

Linear energy analysis

Linear energy analysis is a generalization of the Brønsted plot from classical physical chemistry, where the impact of a mutation on τ_{ON} is compared with K_{eq} (Fersht et al., 1992):

$$\ln\left(\frac{\tau_{ON}^{MT}}{\tau_{ON}^{WT}}\right) = \Phi\left(\ln\left(\frac{K_{eq}^{MT}}{K_{eq}^{WT}}\right)\right) + \text{Const.}$$

For N-type inactivation, which progresses incrementally from one distinct end state to another (Fig. 1 A) (Zhou et al., 2005), provided the mutational effects are modest, such that the reaction still proceeds essentially along the same path, the slope factor, Φ, provides important information about the point along the reaction mechanism that the mutation is impacting. Φ should have a value between 0 and 1 that represents the point during the reaction chain in which the site being mutated is integrated into the inactivated structure, unless the mutation selectively affects an intermediate state, in which case points might fall outside of the region bounded by the 0 and 1 sloped lines.

Online supplemental material

Fig. S1 provides details on the use of elevated K_o to separate N-type inactivation from C-type inactivation in the AKv1 channel, as performed in these experiments. Fig. S1 is available at http://www.jgp.org/cgi/content/full/jgp.200910219/DC1.

RESULTS

Conservation of N-terminal inactivation peptide features

Fig. 2 A shows the alignment of the AKv1 N terminus with N-terminal inactivation domains from several Shaker-type potassium channel subunits, including the classical ShB N terminus and the Kvβ1.1 auxiliary subunit protein N terminus that were the basis for the single-step inactivation and preinactivation models for N-type inactivation (Hoshi et al., 1990; Pfaffinger et al., 1991; Roberds and Tamkun, 1991; Rettig et al., 1994; Ono et al., 1999; Wissmann et al., 2003). These N termini all have a generally nonpolar N terminus (latch region) with high sequence similarity, which has been identified in other studies as the primary location involved in pore binding and thus predicted to be the active site for pore block (Murrell-Lagnado and Aldrich, 1993b; Zhou et al., 2001). After the latch region is a stretch of around six residues (flex region) that is predicted by secondary structure analysis to produce a β turn and is typically highly enriched in glycine residues (Fig. 2 B). Using the alignment in Fig. 2 A, a consensus sequence can be determined for the first 12 residues of the N terminus covering the latch and flex regions. Comparing the consensus to these six sequences, we find that Kvβ1.1 is the least similar (47% similarity) compared with 55% or greater similarly to the consensus for Kv1 α subunits.

The remainder of the N terminus is composed of a region that is generally hydrophilic (polar region).

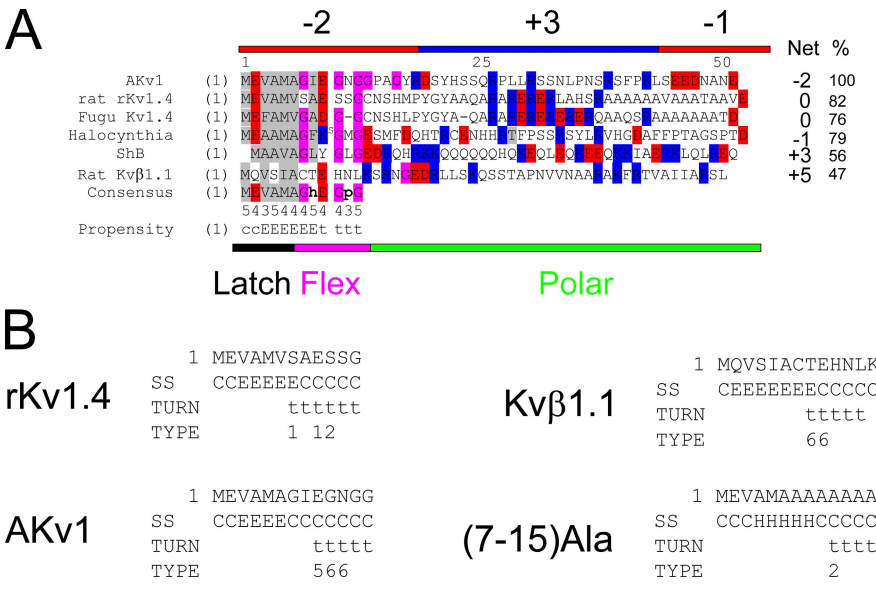

Figure 2. Homology relationships between different Shaker channel N-type inactivation domains. (A) Alignments suggest the partitioning of N terminus into three distinct regions: a hydrophobic latch region, a glycine-rich flex region, and a charged polar region. Specific sequence conservation between N termini is only seen in the latch and flex regions (see Consensus; h, a hydrophobic residue; p, a polar residue). The number below the consensus indicates the number of the six sequences that matches the consensus. Percent identity with consensus ranges from 100% for AKv1 to 47% for Kvβ1.1 (%). Structural prediction for the consensus is given: C, coil; E, extended; t, β turn. Although polar region sequence conservation is low, there is a general charge trend, where this region is predominantly positively charged close to the N terminus but becomes more negative near the T1 domain at the C terminus. Positive charges are not typically found in the latch and flex regions, which typically have a net negative charge. Net charge of N termini varies widely from +5 to −2; however, the general pattern of a more positive N-terminal part of the polar region remains. (B) Structural predictions for selected N termini. General trend for a latch region extended structure and a flex region β turn is present in all N termini but (7–15)Ala, which predicts an α helix at the beginning of the flex region. Turn type code: 1, type I; 2, type II; 3, type VIII; 4, type I' ; 5, type II'; 6, type IV (Fuchs and Alix, 2005).

The N-terminal portion of the polar region is often included as part of the inactivation ball peptide or the preinactivated site, although the primary ascribed function for most of the polar region is to form a flexible but otherwise inert "chain" that tethers the pore-blocking ball region to the channel (Hoshi et al., 1990). Specific sequence conservation is low in the polar region between these different proteins, except for the two Kv1.4 proteins, which display strong polar region sequence conservation despite the enormous evolutionary distance between fish and mammals. Extensive within group similarity of polar region sequences is also apparent in Kvβ1.1 N-terminal sequences that are virtually identical in all mammalian species. This sequence similarity is further evidence for strong evolutionary pressures to conserve polar domain sequences under certain conditions, possibly related to the conservation of unique functional properties within certain gene families.

Despite the presumed importance of positive charges for N-type inactivation, there is no clear overall charge bias for these N termini (Fig. 2 A). In fact, the first 12–14 residues of these N termini, containing the consensus sequence, show acidic residues greatly outnumbering basic residues, resulting in N termini with a median net −2 charge. However, early in the polar region the residue preference switches, with basic residues dominating, producing a large region with a median net +3 charge. By the C-terminal end of the polar region, this charge bias again reverses to an average net −1 charge.

Differential effects of latch and polar region mutagenesis

To map the AKv1 polar region's functional properties, we constructed polyalanine mutants that disrupt portions of the polar region that are normally included in the inactivation ball region, (16–25)Ala, as well as the chain, (36–45)Ala and (46–55)Ala (Fig. 3 A). Previous studies have performed functional mapping

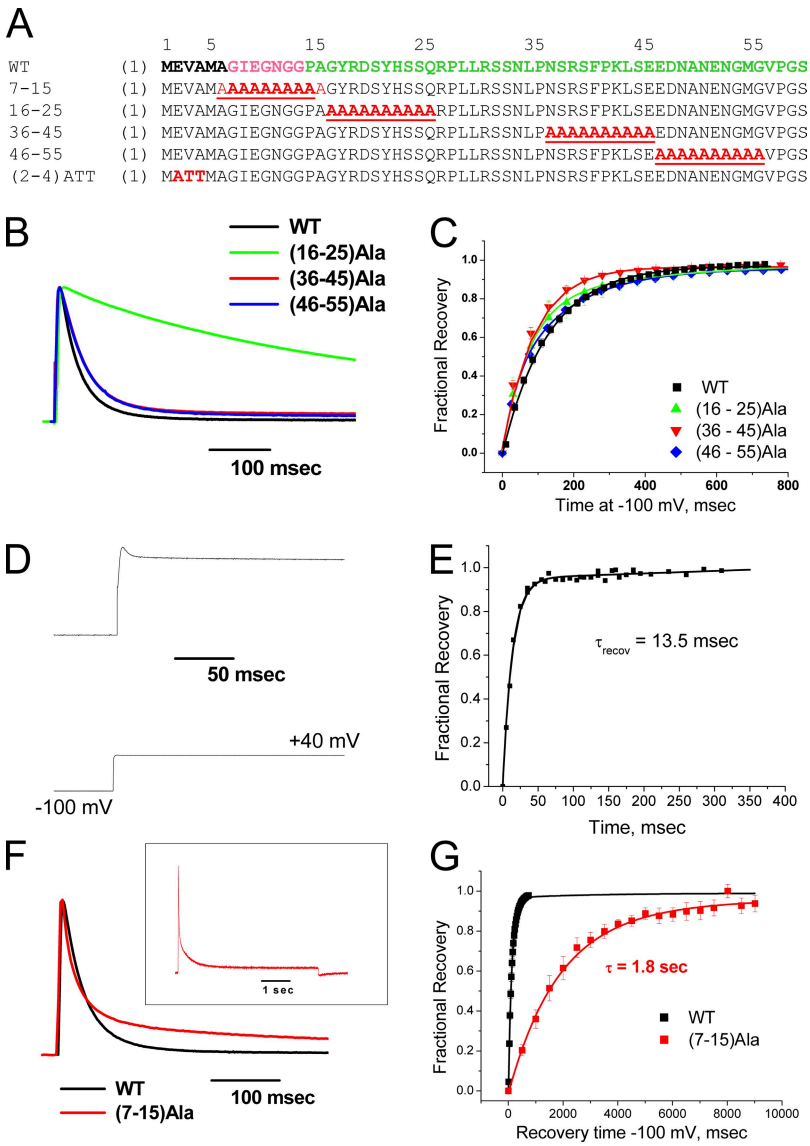

Figure 3. Scanning mutagenesis identifies regions of the N terminus that are important during different phases of N-type inactivation. (A) Wild-type AKv1 N terminus sequences and sequences of scanning mutants made. (B) Polar region scanning mutations slow inactivation with the largest effect produced by (16–25)Ala. (C) Recovery of polar region mutants from inactivation is only slightly different from wild-type, typically showing a slight acceleration. (D) Latch region mutant EVA(2–4)ATT inactivates rapidly but incompletely, resulting in a large sustained current that is not seen in the wild-type channel. (E) Representative experiment showing that recovery from inactivation for EVA(2–4)ATT is accelerated by ∼10 times compared with wild type, as expected for a destabilized binding to the channel pore. (F) Flex region mutation (7–15) Ala produces a pronounced two-exponential inactivation not seen with other mutations. Inset shows inactivation of (7–15)Ala during a 5-s depolarization to +50 mV, emphasizing the slower inactivation kinetic. (G) Recovery of (7–15)Ala from the N-type–inactivated state is dramatically slowed with a time constant ∼14 times slower than wild type.

TABLE I

AKv1 scanning mutations

				Linear energy analysis	
Mutant	Tau on, msec	Tau recovery, msec	K_{eq}	$\Delta\Delta G(\tau_{on})$, kT	$\Delta\Delta G(K_{eq})$, kT
WT	29.5 ± 0.16 (n = 17)	138.8 ± 4.9 (n = 27)	0.21 ± 0.01		
EVA(2-4)ATT	10.7 ± 0.7 (n = 9)[a]	12.8 ± 0.7 (n = 3)[a]	0.84 ± 0.07[a]	−1.01 ± 0.07	1.37 ± 0.09
7-15 Ala (f)	21.4 ± 1.6 (n = 5)[b]	1551 ± 103 (n = 3)[a]	0.01 ± 0.001[a]	−0.32 ± 0.07	−2.73 ± 0.11
7-15 Ala (s)	335.7 ± 21.6 (n = 5)[a]	1551 ± 103 (n = 3)[a]	0.22 ± 0.02	2.43 ± 0.06	0.02 ± 0.10
16-25 Ala	504.9 ± 30.8 (n = 4)[a]	103.7 ± 30.8 (n = 4)[b]	4.63 ± 0.51[a]	2.84 ± 0.06	3.13 ± 0.31
36-45 Ala	43 ± 2.9 (n = 5)[a]	82.7 ± 8.2 (n = 5)[a]	0.52 ± 0.06[a]	0.38 ± 0.07	0.89 ± 0.13
46-55 Ala	52.3 ± 2 (n = 6)[a]	105 ± 4.2 (n = 3)	0.50 ± 0.12[a]	0.57 ± 0.04	0.85 ± 0.07

[a]$P < 0.01$ and [b]$P < 0.05$ compared to wild type.

of the N terminus using deletion analysis; however, this method has the disadvantage of changing both the backbone length as well as the side chain properties at a given registration from the N terminus or T1 domain, making this approach difficult to interpret (Hoshi et al., 1990; Wissmann et al., 2003). Summary results are presented in Table I. The most N-terminal polar region substitution, (16–25)Ala, produced a dramatic >15-fold slowing of inactivation compared with wild-type AKv1 (Fig. 3 B), suggesting that in spite of the relatively low level of sequence conservation in this region, it is playing an important role in N-type inactivation. Both (36–45)Ala and (46–55) Ala also slowed the inactivation time course, but the effect was more modest, amounting to around a 1.5-fold slowing. Interestingly, none of these substitutions had a large effect on recovery from inactivation (Fig. 3 C).

To compare these effects to a mutation in an inactivation ball segment that is proposed to bind within the pore, we introduced the EVA(2–5)ATT substitution, which changes the polar nature of three residues in the latch region (Fig. 3 A). Interestingly, this mutant shows a rapid inactivation time course; however, it also dramatically reduces the extent of inactivation, resulting in a large sustained current (Fig. 3 D). The phenotype of this mutant, rapid inactivation gate closing but failure to remain shut, provided the inspiration for naming this region of the inactivation gate the "latch" region. The fraction of current that is inactivated recovers very rapidly, ∼10 times faster than normal, consistent with a mutation that lowers the affinity of binding within the pore (Fig. 3 E).

Linear energy analysis of latch and polar scanning mutations

The fact that our latch region mutation had a large effect on recovery kinetics, whereas the polar region mutations did not, suggests that these regions of the N terminus are unbinding from the inactivated structure at different times during the recovery process. To better quantify these differences, we performed linear energy analysis (Table I) to compare the energetic impact of mutations on the reaction equilibrium (K_{eq}) versus their effect on the adjusted time constant to inactivation (τ_{ON}) (Fig. 4) (Fersht et al., 1992; Zhou et al., 2005). Here, we find that the three polar region mutations plot very close to the Φ = 1 line, suggesting that they integrate into the inactivated structure early in the inactivation reaction. In contrast, the EVA(2–4)ATT mutation plots outside the normal region bounded by the Φ = 1 (Fig. 4, black) and Φ = 0 (red) lines, suggesting both a catalytic effect as well as a reduction in affinity for the bound state of the N terminus. This plot location in a negative slope region is independent of whether EVA

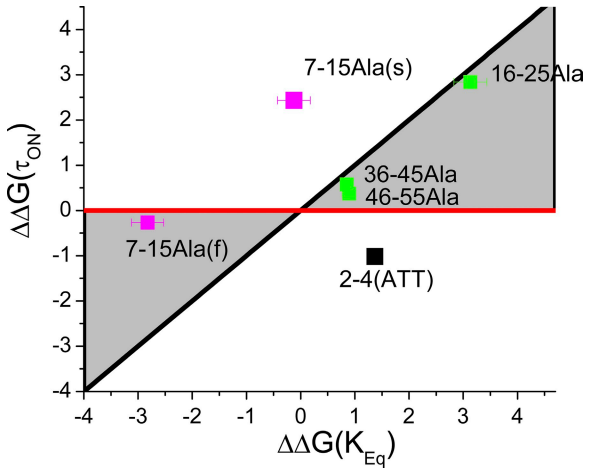

Figure 4. Linear energy analysis of N-terminal mutants predicts differential consolidation into inactivated structure. Table I values for energetic effects of mutations on τ_{on} and K_{eq} are plotted. Linear energy plot shows that polar region mutations have their primary effect early in the inactivation cycle because they plot near the Φ =1 line (Black). (7–15)Ala channels inactivating with the fast kinetic plot near the Φ = 0 line (red), suggesting that a later step in the inactivation process is impacted by this mutation in these channels. (7–15)Ala channels inactivating with a slow kinetic likely reflect channels that do not reach transition normally because they plot outside the normal, grayed out region of the linear energy plot. There is almost no effect on K_{eq}, suggesting a similar impact of this mutation on both ON and recovery reactions. EVA(2–4)ATT also plots outside the normal region of the linear energy plot but shifts to the right, indicating a greater impact on recovery, suggesting a later impact of this mutation in addition to its effect on the intermediate transition reaction.

(2–4)ATT is analyzed by a two- or three-state model and is evident in the data by the fact that this mutation accelerates both inactivation at positive potentials and recovery at negative potentials. EVA(2–4)ATT is a later-acting mutation compared with polar region mutations because the additional effect of this mutation, beyond the catalytic effect, is only evident on recovery.

Flex region mutational analysis

To compare our results on the latch and polar region mutations to mutagenesis of the intervening flex region, we disrupted the entire flex region with a (7–15)Ala substitution (Fig. 3 A) and examined the effects on inactivation and recovery. The (7–15)Ala mutant dramatically impacts both the inactivation and recovery processes in different ways. The inactivation on kinetic converted from a single-exponential process to a strikingly two-exponential process, with the faster kinetic 25% faster than normal. The slower kinetic process produces inactivation ∼11 times slower than normal, but still around 10 times faster than C-type inactivation in elevated extracellular K^+ (Fig. 3 F; compare with Fig. S1 D). Recovery is also dramatically slowed by around 14 times, but interestingly, other than residual C-type recovery, recovery from N-type inactivation is single exponential with both the fast- and slow-inactivation components of (7–15)Ala recovering together (Fig. 3 G). This suggests that a common N-type–inactivated state is being formed during the inactivation processes.

We performed linear energy analysis on the (7–15)Ala substitution by plotting the fast and slow kinetics separately (Table I). Fig. 4 shows that channels inactivating by the faster inactivation kinetic plot very close to the $\Phi = 0$ line, indicating that for these channels, the (7–15)Ala mutation primarily has an impact late in the reaction mechanism, well after the rate-limiting step. The more slowly inactivating kinetic, however, plots outside the normal plot region, shown in Fig. 4 in gray, indicating that these channels have a problem transitioning normally.

Electrostatic interactions involving polar region 16–25

Previous studies on the ShB inactivation domain showed that the pore-blocking efficacy of peptides made from the ShB N terminus increases with the addition of positive charges anywhere in the C-terminal end of the peptide (Demo and Yellen, 1991). This suggested that these positive charges are sensing a diffuse negative steering potential that attracts the blocking particle into the pore regardless of the specific residue that is made positive. A diffuse steering potential effect cannot explain our results because the (16–25)Ala mutation, which has the largest effect, produces no net change in N-terminal charge. To test if specific electrostatic interactions play any role in (16–25)Ala mutation's functional effect, we individually mutated the single-positive charge, R18, and single-negative charge, D19, which are located within the 16–25 region. Both charge-neutralizing mutations R18A and D19A, as well as charge-reversing mutations to R18E or D19K, were introduced to test for electrostatic effects (summary results in Table II). As can be seen in Fig. 5 A, changing the charge on residue 18 has a dramatic effect on the inactivation kinetics, with a >10-fold slowing of inactivation after switching from a positive to a negative charge at this site. Consistent with our previous observations with (16–25)Ala, charge-changing mutations at residue 18 had little effect on recovery from inactivation (Fig. 5 B). In contrast to the >10-fold effects of charge change on inactivation kinetics produce by residue 18, changing the charge at the neighboring residue 19 from negative to positive

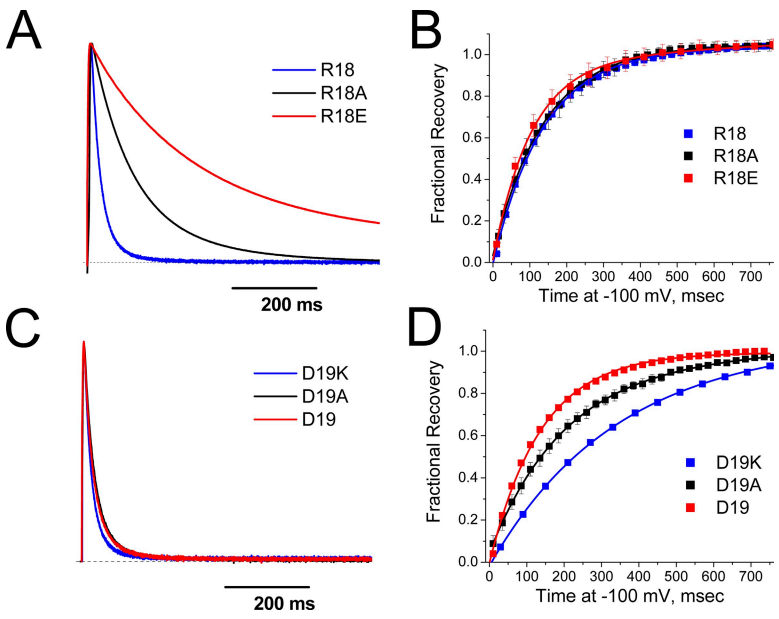

Figure 5. Functional effects of changing charges in the 16–25 segment of the polar region. Charged residues R18 and D19 were systematically mutated from (positive, zero, negative) charge to determine the magnitude of the electrostatic potential changes these residues experience during N-type inactivation. (A) Inactivation slows as position 18 is made more negative from its normal positive charge. (B) Recovery from inactivation shows little sensitivity to charge at position 18. (C) Inactivation accelerates slightly as position 19 is made more positive from its normal negative charge. (D) Recovery shows a greater sensitivity to charge at position 19, becoming slower as position 19 is made more positive. The results suggest that both positions 18 and 19 experience a negative potential change between the free and bound states, but the magnitude and phase vary between the two residues.

TABLE II

Polar region charge-changing point mutations

				Linear energy analysis	
Mutant	Tau on, msec	Tau recovery, msec	K_{eq}	$\Delta\Delta G(\tau_{on})$, kT	$\Delta\Delta G(K_{eq})$, kT
WT	29.5 ± 0.16 (n = 17)	138.8 ± 4.9 (n = 27)	0.21 ± 0.01		
R18A	98 ± 3.8 (n = 12)[a]	123 ± 5.6 (n = 5)[b]	0.80 ± 0.05[a]	1.20 ± 0.04	1.32 ± 0.07
R18E	401.6 ± 15.7 (n = 16)[a]	127.4 ± 5.6 (n = 15)[a]	3.15 ± 0.18[a]	2.61 ± 0.04	2.70 ± 0.07
D19A	29.6 ± 0.9 (n = 7)	232.4 ± 12 (n = 8)[a]	0.13 ± 0.01[a]	0.00 ± 0.03	−0.51 ± 0.07
D19K	22.5 ± 0.8 (n = 7)[a]	355.5 ± 6.2 (n = 5)[a]	0.06 ± 0.003[a]	−0.27 ± 0.04	−1.21 ± 0.05
R26A	47.6 ± 3.3 (n = 9)[a]	106 ± 8 (n = 9)[a]	0.45 ± 0.05[a]	0.48 ± 0.07	0.75 ± 0.11
R30A	47.6 ± 2.3 (n = 9)[a]	100.7 ± 4.2 (n = 9)[a]	0.47 ± 0.03[a]	0.48 ± 0.05	0.80 ± 0.07
R38A	42.3 ± 1.3 (n = 11)[a]	116 ± 6.5 (n = 8)[a]	0.36 ± 0.02[a]	0.36 ± 0.03	0.54 ± 0.07
K42A	41.6 ± 2.4 (n = 10)[a]	103.9 ± 5.1 (n = 10)[a]	0.40 ± 0.03[a]	0.34 ± 0.06	0.63 ± 0.08
E45A	26.8 ± 2.6 (n = 4)	106.4 ± 12 (n = 4)	0.25 ± 0.04	−0.10 ± 0.10	0.17 ± 0.15
E46A	21.2 ± 0.6 (n = 8)[a]	152.5 ± 5.9 (n = 8)[b]	0.14 ± 0.01[a]	−0.33 ± 0.03	−0.42 ± 0.06
E46K	31.3 ± 1.3 (n = 7)	175.5 ± 0.8 (n = 7)[a]	0.18 ± 0.01[a]	0.06 ± 0.04	−0.17 ± 0.05
D47A	40 ± 1.5 (n = 6)[a]	117 ± 2.5 (n = 5)[a]	0.34 ± 0.01[a]	0.30 ± 0.04	0.47 ± 0.06
E51A	28.6 ± 4.3 (n = 5)	144.5 ± 9.5 (n = 5)	0.20 ± 0.03	−0.03 ± 0.15	−0.07 ± 0.17

[a]$P < 0.01$ and [b]$P < 0.05$ compared to wild type.

only accelerated the inactivation kinetics by around 25% (Fig. 5 C). In fact, a significantly larger effect was observed on recovery from inactivation, where replacing the native residue 19 negative charge with a positive charge slows recovery by >2.5-fold (Fig. 5 D).

We can better compare the relative impact of these charge-changing mutations by plotting pseudo first-order energy-binding curves using the time constants to inactivate and recover to estimate the rate-limiting energy jumps for the binding and unbinding reactions. To compare these plots, we assume that the free-state energy has not been significantly altered and thus assign the free state a relative energy of 0 kT. In Fig. 6 A, we plot the predicted energy state diagrams for channels that are identical except for the charge at position 18. The results show a very consistent impact of charge change with a similar energetic difference between R18E and R18A as there is between R18A and R18 at the transition and bound states. Consistent with our other results, the differential impact of charge is primarily on the energy between the free and transition states, which controls the time constant for inactivation. If we plot the change in transition- or bound-state energy versus the charge at position 18, we get linear relationships consistent with an electrostatic effect (Fig. 6 B). For the transition state, the slope of this line is 1.18 kT units per charge change, predicting an electrical potential drop of −30.7 mV experienced at position 18 between the free and transition states. As expected, the results are similar for the bound state, with a predicted potential drop between the free and bound states of −32.7 mV.

In Fig. 6 C, we plot the predicted energy state diagrams for channels that are identical except for the charge at position 19. The results again show a very consistent impact of charge change in the same direction as position 18; however, the shift at the transition state is much smaller and there is a larger change between transition and bound. Interestingly, despite their native opposite charges, comparing the energy-state diagrams for positions 18 and 19, Fig. 6 (A and C) suggests that the native residues R18 and D19 may work together to increase the speed of the inactivation gating cycle, with R18 accelerating inactivation with little effect on recovery, and D19 accelerating recovery with little effect on inactivation. To determine the electrostatic potential changes experienced at residue 19 during the inactivation process, in Fig. 6 D we plot the energies of the transition and bound states versus charge at residue 19. The slope of the ON transition line suggests a very small change in potential experienced at residue 19 of −3.5 mV. At the bound state, the predicted potential difference from free at residue 19 is −15.5 mV, a −12-mV change from transition, but still less that half that experienced by residue 18.

Electrostatic interactions throughout the polar region

In the remainder of the AKv1 polar region, after residue 25, there are eight charged residues with a strong bias for positive charges closer to the N terminus and negative charges closer to the C-terminal link to the T1 domain (Fig. 2 A). Although the (26–35)Ala and (46–55) Ala mutations had smaller effects on inactivation than (16–25)Ala, this pattern of charge conservation suggests that other polar region charges may be playing an important electrostatic role in regulating N-type inactivation. To address this question, point mutations were performed on the remainder of the charged residues in the polar region (summary results in Table II).

Neutralization of positive charges R26, R30, R36, or K42 slowed inactivation similar to R18A, but the effect

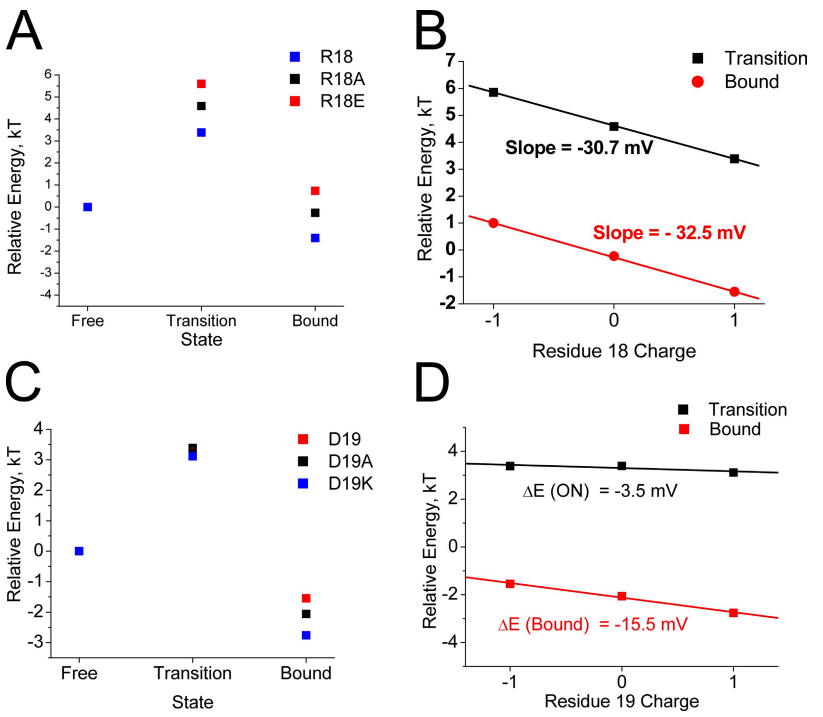

Figure 6. Inactivation reaction energetics predict that a negative electrostatic potential change is experienced by residues 18 and 19 during N-type inactivation. Energy state diagrams are constructed based on the effects of charge-changing mutations at residues 18 and 19 on the ON and recovery reactions. Free-state energy level is assumed to be unaffected by mutations and is set to 0. (A) Progressively higher transition-state energy as position 18 is made more negative suggests a negative electric field experienced by this residue during inactivation. There is no significant further effect between transition and the bound state. (B) Change in energy plotted versus the charge at position 18. Energy change is linear as expected for an electrostatic effect, with the slope of the line giving the potential change experienced by position 18 from the free state to either the transition or bound states. (C) Residue 19 mutations show a greater impact on recovery than inactivation, unlike other polar region mutations. Energy levels increase for more negative charges at residue 19, again suggesting a negative potential change during inactivation. (D) The effects of charge-changing mutations at residue 19 are linear for both inactivation and recovery, suggesting that D19 is primarily interacting electrostatically with the channel core. The net potential change experienced by D19 during binding is less than half that experienced by R18, suggesting significant local heterogeneity in experienced potential changes. The late effect of residue 19 mutations, after the ON transition state, may indicate that this residue is pointed away from the channel polar region binding surface and thus is not directly involved in polar region binding to the channel, but rather primarily affects how the latch and flex regions enter and exist from the pore block site.

was smaller, around 1.5-fold (Fig. 7 B). None of these mutations had a large effect on recovery, with at most a 25% acceleration of recovery (Fig. 7 C). If we plot the predicted electrical potential change experienced at these sites during inactivation versus the position mutated, we see that all these positive charges are experiencing a negative potential change during the ON reaction before reaching the transition state, but relatively little potential change during recovery (Fig. 7, D and E).

Given the consistent results of a negative electric field sensed by the positive charges, we were interested in determining if the same results would be obtained with the negative charges located nearer the T1 domain. Similar measurements to those performed on positive charges in Fig. 7 (B–E) were performed on the four negative charges E45, E46, D47, and E51. The estimated energy of the bound state compared with free is plotted versus the charge at each position and compared with our previous results on D19 (Fig. 7 F). Interestingly, the negatively charged residues closer to the T1 domain did not report a significant negative potential change during inactivation. For positions 45, 46, and 51, the energetics of the bound state were not significantly affected by charge-changing mutations (Fig. 7 E). Position 47, in contrast, destabilized the bound state when its negative charge was neutralized, suggesting that this site may be experiencing a positive potential change of as much as 15 mV during N-type inactivation. The combined data for all the residues tested in the polar region show a clear overall trend in which the experienced electric field becomes progressively more negative for positions closer to the N terminus (Fig. 7 G). This electric field gradient is complementary to the acidic to basic trend in polar region–charged residues occurring over the same region (Fig. 2 A).

Energetic coupling to side window residues

Our results suggest that even for polar residues located far from the inactivation site, the electrostatic interactions they experience appear to be very position specific, as if they are involved in forming precise interactions to the surface of the channel. If such a polar region–binding site is present on the surface of the channel, we should see evidence of this by thermodynamic mutant cycle analysis between the N terminus and the channel core. Based on the crystal structure of the Kv1.2 channel, EM reconstructions, and mutational analyses, it is proposed that the pore-blocking region of the N terminus must enter "side windows" located between the T1 domain and the channel core to reach the transmembrane pore where block occurs (Gulbis et al., 2000; Sokolova et al., 2001; Zhou et al., 2001; Long et al., 2005; Wang et al., 2007). Therefore, an important question is whether there is energetic coupling between the AKv1 polar region and residues located in the side windows of the channel. For this study, we chose to

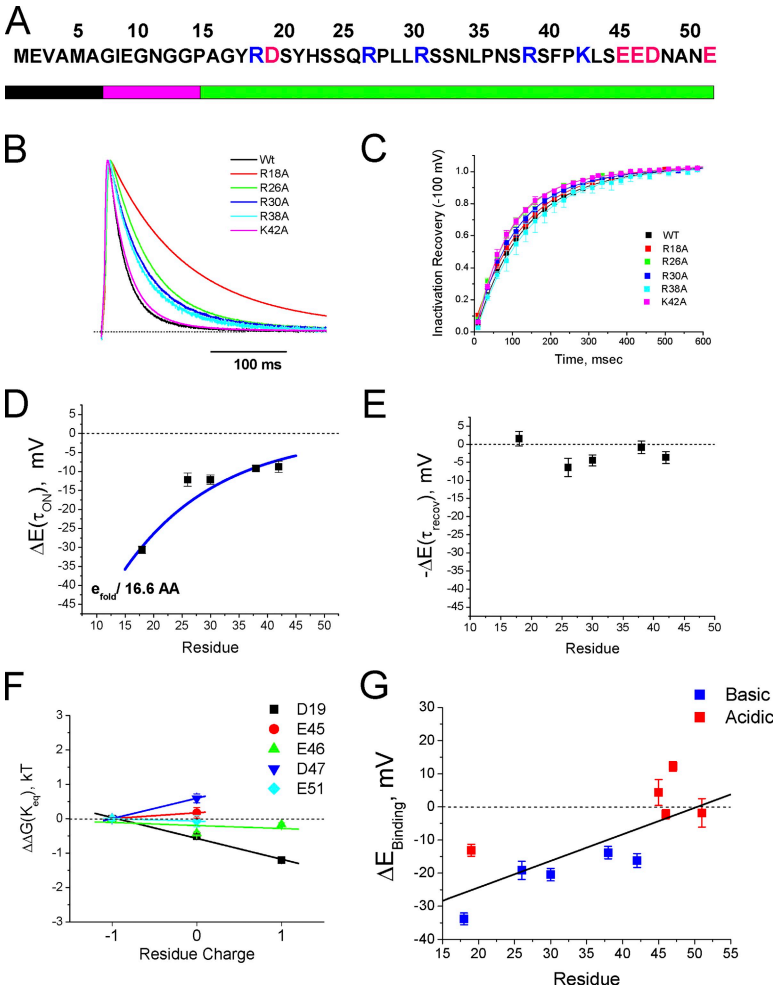

Figure 7. Electrostatic interactions occur throughout the polar region. (A) Location of charged residue within the polar region of the AKv1 N terminus. (B) Neutralization of positive charges by mutation to alanine produces a slowing of inactivation that becomes progressively bigger as the mutations are made closer to the N terminus. (C) Neutralizing positive charges has little effect on recovery from inactivation. (D) Estimated potential change experienced by these residues upon binding. Largest change is an ~30-mV change for position 18. Slow decay in potential (e-fold per 16.6 residues) is less than what would be predicted for a single site acting from a region near the pore on an unstructured chain with a Debye length of ~9 Å for frog Ringer. (E) No significant effect of position on potential change experienced during recovery suggests that all the potential change experienced during binding occurs after the transition state for recovery. (F) A series of mutations to normally negative residues in the polar region of the N terminus. Slope of line indicates the sign and strength of the electric field change experienced at this site between the free and bound states. Biggest positive potential change is experienced by residue 47, with only residue 19 experiencing a large negative potential change. (G) Summary plot showing the potential changes experienced by charges in the polar region during N-type inactivation. Results show a strong trend with more negative potentials experienced in regions dominated by positively charged residues. D19 experiences a strong negative potential, but this potential is in a local minimum compared with the adjacent R18 and R26.

examine side window residues EDE(161–3), located in the outer part of the side windows, and V135, located deep in the side windows pointing toward the transmembrane pore. Although V135 is not normally charged, its location immediately beneath the pore allows us to probe how deeply the polar region enters the channel during N-type inactivation. These sites are also homologous to residues identified in rKv1.4 as forming preinactivation site interactions with the Kvβ1.1 N terminus (Gulbis et al., 2000; Zhou et al., 2001). Charge-changing mutations EDE(161–3)KKK and V135K were constructed and examined for energetic interactions with polar region–charged residues using mutation cycle analysis. On its own, the mutation EDE(161–3)KKK dramatically slowed the inactivation time course (10 times slower) as well as the recovery time course (2 times slower), whereas the V135K mutation only modestly accelerated inactivation by ~25% with little effect on recovery (Table III).

We then characterized the energetic coupling coefficient Ω for the inactivation ON and recovery reactions between these two channel core sites and polar region–charged residues (Fig. 8 and summary results in Table III). For core residues 161–3, a large selective coupling interaction was observed during the inactivation ON reaction between residue 18 and 161–3 (Fig. 8 A). The large difference in coupling coefficient for residue 18 compared with other charged residues, including the adjacent residue 19, suggests a specific binding interaction between position 18 and the 161–3 region of the channel core. The failure to observe coupling between these sites during recovery again suggests that the interactions residue 18 forms with the channel are made early in the inactivation process, before reaching the transition state, and do not reverse until late in the recovery process, after the rate-limiting step is passed.

For the more centrally located residue 135, there was no selective coupling between any specific charged residue in the polar region and this site (Fig. 8 B). This suggests that unlike 161–3, charged residues in the polar region are not selectively interacting with residue 135. Interestingly, although there is no specific interaction of N-terminal residues with residue 135, this site does appear to provide a weak diffusive electrostatic steering potential that is felt by several polar region residues, falling off with distance from the N terminus around e-fold per

TABLE III

Mutant cycle analysis

Mutant	Tau on, msec	Tau recovery, msec	Ω (On)	Ω (Recov)
V135K	22.8 ± 1.3 (n = 12)[a]	134.8 ± 4.4 (n = 12)		
V135K/R18A	61.8 ± 0.89 (n = 4)[a]	150.8 ± 2.8 (n = 4)[a]	1.6 ± 0.1	1.2 ± 0.1
V135K/D19A	34.3 ± 0.97 (n = 4)[a]	177.2 ± 4.8 (n = 4)[a]	1.5 ± 0.1	1.3 ± 0.1
V135K/R26A	27.3 ± 0.8 (n = 7)[a]	94.4 ± 2.9 (n = 7)[a]	1.2 ± 0.1	1.0 ± 0.1
V135K/R30A	33.2 ± 0.8 (n = 6)[a]	92.5 ± 2.1 (n = 5)[a]	1.1 ± 0.1	1.1 ± 0.1
V135K/R38A	33.4 ± 1.4 (n = 5)[a]	110.4 ± 4.4 (n = 5)[a]	1.0 ± 0.1	1.0 ± 0.1
V135K/K42A	33.3 ± 2.2 (n = 5)[a]	105 ± 10 (n = 3)	1.0 ± 0.1	1.0 ± 0.1
EDE/KKK	321 ± 9.5 (n = 16)[a]	286.5 ± 12.4 (n = 13)[a]		
KKK/R18A	465.7 ± 15.4 (n = 9)[a]	328.2 ± 14.2 (n = 4)	2.3 ± 0.2b	1.2 ± 0.1
KKK/D19A	367.9 ± 15 (n = 7)[a]	318 ± 13.7 (n = 8)[b]	1.1 ± 0.1	1.5 ± 0.1
KKK/R26A	345 ± 7.6 (n = 3)	286.3 ± 13.7 (n = 3)	1.5 ± 0.1	1.3 ± 0.1
KKK/R30A	402.4 ± 14 (n = 6)[a]	264.25 ± 13 (n = 6)	1.3 ± 0.1	1.3 ± 0.1
KKK/R38A	353 ± 9 (n = 8)[a]	277.4 ± 12.7 (n = 8)	1.4 ± 0.1	1.2 ± 0.1
KKK/K42A	349.7 ± 15.5 (n = 5)	309.7 ± 20 (n = 5)	1.3 ± 0.1	1.4 ± 0.1

[a]$P < 0.01$ and [b]$P < 0.05$. Mutants compared to V135K or EDE(161-3)KKK parent constructs, respectively; EDE(161-3)KKK or V135K constructs compared to wild type.

10 residues. The observed coupling with residue 135 is selective for the on process for all residues but residue 19, which also shows some coupling during recovery.

Analysis of electrostatic interactions between the channel core and residue 18

To determine if the identified specific coupling between position 18 and 161–3 represents an electrostatic interaction between these sites, we tested if the potential experienced by position 18 during inactivation changes in a linear manner with the charge at position 161–3 (summary results in Table IV). In Fig. 9 A, we plot the energy jump to reach the ON transition state versus the residue 18 side chain charge for different substitutions at position 161–3. The EDE plot is identical to the plot from Fig. 6 B, and it shows the sensitivity of the ON inactivation reaction to the charge at position 18 for the channel with the native EDE residues at position 161–3. As discussed previously, the energy to reach the transition state drops dramatically, in a linear manner, when position 18 is made more positive due to the −30-mV drop in potential experienced by residue 18 between the free and transition states. The plot labeled AAA shows the same experiment only with the residues at position 161–3 neutralized to alanines. As before, the energy to reach the transition state decreases in a linear manner as position 18 is made more positive; however, the effect is significantly less. The weaker impact of residue 18 mutations suggests that the negative potential being experienced by position 18 decreases when position 161–3 is neutralized. Finally, the plot labeled KKK shows that the energy to reach the transition state is almost insensitive to the charge placed at position 18 when residues 161–3 are changed to positive lysine residues.

To determine the magnitude of the potential produced by residue 161–3 at the site reached by residue 18 during polar region binding, we need to compare how the apparent potential sensed by residue 18 changes with the charge present at the 161–3 site. As discussed previously, the potential sensed by residue 18 is given by the slope of the line relating transition energy to

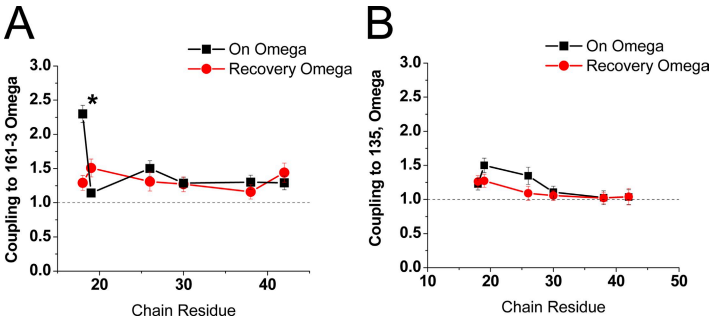

Figure 8. Mutant cycle analysis between polar region residues and channel charges located near side windows. 161–3 is located at the periphery of the side windows, whereas 135 is located with the side windows at the axis of symmetry. We examined the impact of interactions between these channel residues and the polar region sites on the rate-limiting transitions for inactivation ON and recovery reactions. (A) The interaction between residues 18 and 161–3 during the ON process is the only one significantly different from all the others (indicated by *). Adjacent residue 19 has no significant interaction with 161–3, suggesting that the interaction with position 18 is specific and that residue 19 likely is pointed away from 161–3. (B) No residue shows a strong specific interaction with position 135. Coupling is greatest to D19 during the ON process, and it seems to fall off steadily with distance, suggestive of a diffuse electrostatic effect. Failure to see specific coupling suggests that the polar region does not reach far into the side windows during inactivation, but that D19 may be oriented toward the side window opening.

TABLE IV

Residue 18 coupling potential analysis

Mutant	Tau on, msec	Tau recovery, msec	$\Delta G(\tau_{on})$, kT	$\Delta G(\tau_{recov})$, kT	On slope, $\Delta kT/(+)$	Recov slope, $\Delta kT/(+)$
V135K/R18	22.8 ± 1.3 (n = 12)[a]	134.8 ± 4.4 (n = 12)	3.13 ± 0.06	4.90 ± 0.03		
V135K/R18A	61.8 ± 0.89 (n = 4)[a]	150.8 ± 2.8 (n = 4)[a]	4.12 ± 0.01	5.02 ± 0.02	−0.96	−0.22
V135K/R18E	117.6 ± 8.6 (n = 3)[b]	168 ± 21 (n = 3)	4.80 ± 0.07	5.12 ± 0.13		
V135/R18	29.5 ± 0.16 (n = 17)	138.8 ± 4.9 (n = 27)	3.38 ± 0.01	4.93 ± 0.04		
V135/R18A	98 ± 3.8 (n = 12)[a]	123 ± 5.6 (n = 5)[b]	4.58 ± 0.04	4.81 ± 0.05	−1.28	−0.05
V135/R18E	401.6 ± 15.7 (n = 16)[a]	127.4 ± 5.6 (n = 15)[a]	6.00 ± 0.04	4.85 ± 0.04		
V135D/R18	39.2 ± 1.5 (n = 3)[a]	166.4 ± 6.5 (n = 3)[a]	3.67 ± 0.04	5.11 ± 0.04		
V135D/R18A	258 ± 15.2 (n = 10)[a]	133.3 ± 7 (n = 9)[b]	5.55 ± 0.06	4.89 ± 0.05	−1.63	−0.20
V135D/R18E	1006 ± 75 (n = 10)[a]	116.8 ± 2.7 (n = 10)[b]	6.91 ± 0.07	4.76 ± 0.02		
KKK/R18	321 ± 9.5 (n = 16)[a]	286.5 ± 12.4 (n = 13)[a]	5.77 ± 0.03	5.66 ± 0.04		
KKK/R18A	465.7 ± 15.4 (n = 9)[a]	328.2 ± 14.2 (n = 4)	6.14 ± 0.03	5.79 ± 0.04	−0.14	0.00
KKK/R18E	428 ± 16.7 (n = 6)[a]	289 ± 13 (n = 6)	6.06 ± 0.04	5.67 ± 0.04		
AAA/R18	44.5 ± 0.8 (n = 3)[a]	152.5 ± 7.4 (n = 3)[a]	3.80 ± 0.02	5.03 ± 0.05		
AAA/R18A	101.8 ± 4 (n = 6)[a]	208.1 ± 9.9 (n = 6)[a]	4.62 ± 0.04	5.33 ± 0.05	−0.53	−0.13
AAA/R18E	113.9 ± 4 (n = 6)[a]	203.4 ± 4.5 (n = 6)[b]	4.74 ± 0.04	5.32 ± 0.02		
EDE/R18	29.5 ± 0.16 (n = 17)	138.8 ± 4.9 (n = 27)	3.38 ± 0.01	4.93 ± 0.04		
EDE/R18A	98 ± 3.8 (n = 12)[a]	123 ± 5.6 (n = 5)[b]	4.58 ± 0.04	4.81 ± 0.05	−1.28	−0.05
EDE/R18E	401.6 ± 15.7 (n = 16)[a]	127.4 ± 5.6 (n = 15)[a]	6.00 ± 0.04	4.85 ± 0.04		

[a]$P < 0.01$ and [b]$P < 0.05$. R18 mutants compared to V135K or EDE(161-3)KKK parent constructs, respectively; R18 plus EDE(161-3)KKK or V135K constructs compared to wild type.

residue 18 charge. If we plot these slopes for the different substitutions at position 161–3 versus the charge at position 161–3, the dependence of the slope on the charge at 161–3 can be determined (Fig. 9 E). As expected for a purely electrostatic interaction between residue 18 and 161–3, these slopes change in a linear manner dependent on the charge at 161–3, suggesting that position 18 feels an electrical potential of −14.7 mV coming from EDE(161–3) (or +14.7 mV from KKK(161–3)) when the transition state is attained. This is equivalent to half the total potential change felt by residue 18. If we perform the same analysis on the recovery energetics, we see a very small change in the electrostatic interaction between R18 and EDE(161–3) equivalent to 0.6 mV, suggesting that there is little change in the relationship between R18 and EDE(161–3) during recovery as the N terminus progresses from the fully inactivated state back to transition (Fig. 9 E).

We also tested for the magnitude and electrostatic nature of the diffusive electrostatic coupling between position 18 and 135 (summary results in Table IV). In Fig. 9 C we show the sensitivity of the ON transition-state energy to changes in position 18 charge depending on the charge at residue 135. The V135 plot is the wild-type plot and thus is identical to the wild-type plot in Fig. 6 B and to the EDE plot in Fig. 9 A. Because V135 is uncharged, it normally does not interact electrostatically with position 18; however, we can test whether residue 18 can sense an electrostatic potential produced by position 135 by introducing charges into position 135. Because residue 135 is at the central axis of the channel, a single substitution here produces a change in four charges at the central axis of the channel. Substitution of a negative charge into residue 135, V135D, does make the inactivation ON transition-state energy more sensitive to the charge at position 18 than the wild-type channel. A steeper, linear decrease in transition-state energy as residue 18 is made more positive suggests that position V135D adds to the electrostatic field that is attracting position 18 to its binding site during the inactivation on reaction. Introducing the opposite charge at residue 135, V135K, reduces the sensitivity of the ON transition-state energy to the charge at position 18. As we have previously seen for all residue 18 mutations, there is little effect of any of these mutations on the recovery process (Fig. 9 D). If we plot the change in slope for the ON reaction energy produced by residue 18 substitutions versus the charge at residue 135, we see that R18 feels an electrical potential of around −8.5 mV coming from position 135 as the polar region binds to the channel in the presence of the V135D substitution (or +8.5 from V135K) (Fig. 9 F). In agreement with our previous studies, there is very little change in the relationship between residues 18 and 135 (0.2 mV), as recovery progresses from the fully inactivated state back to the transition state (Fig. 9 F).

Linear energy analysis of polar region point mutations

Preliminary deca-alanine scanning experiments (Figs. 3 and 4) suggested that the polar region integrates into its final location in the inactivated structure early in the inactivation process before the rate-limiting step.

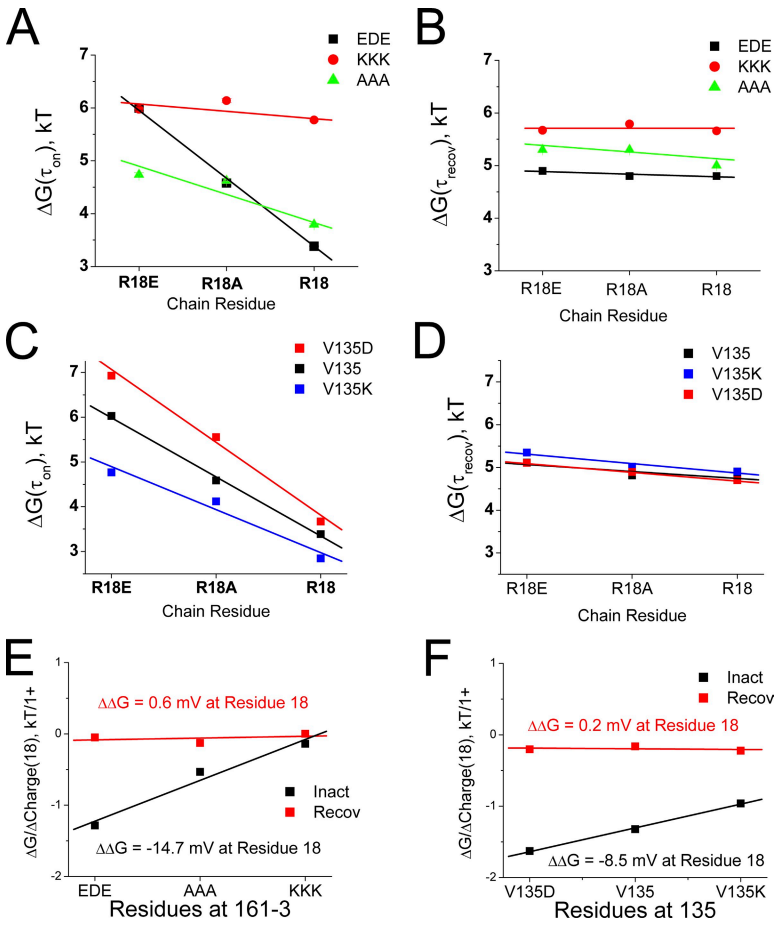

Figure 9. Analysis of the importance of electrostatics for interactions between residue 18 and the side window residues 161–3 and 135. Charge-changing mutations were made in both the side window location and in residue 18, and the energetic effect on the rate-limiting inactivation ON and recovery reactions was determined. (A) Changing residue 18 charge alters the energetics of the inactivation on reaction in a linear manner. The slope changes depending on the charge present at residues 161–3. As 161–3 is made more positive, the energetic impact of changing residue 18 charge is lost, indicating a large electrostatic contribution of 161–3 on the potential change felt by residue 18. (B) There is little impact on recovery of charge changes to residue 18, and the slopes of these lines do not change much with changes in the charge at residues 161–3. (C) Charge at residue 135 has a similar effect on slope as residue 161–3, but the impact is less pronounced. Because residue135 is at the axis of symmetry, four net charges in the center of the side windows are changed with each residue 135 mutation; however, the number of these charges that are seen by residue 18 is unknown. (D) As expected, energetic coupling shows little charge dependence for residue 18 and 135 between the bound and transition state during recovery. (E) Summary diagram for coupling between residue 18 and 161–3. As expected, there is no significant change in electrostatic interaction between residue 18 and 161–3 during the recovery process, but there is a large potential change produced during inactivation as the polar region binds. The potential produced by EDE(161–3) is ∼−15 mV, about half the total potential change seen by residue 18. (F) Coupling between residue 18 and 135 shows a similar pattern with no change in interaction during recovery, but an estimated −8.5-mV change on binding (with V135D). Because curves are almost perfectly linear, it suggests that there is no significant non-electrostatic interaction between residue 18 and residue 135. Because residue 135 is normally uncharged, this interaction has no impact on inactivation in the wild-type channel.

To extend these analyses and test if all charged residues in the polar region of the N terminus coalesce into their final locations early in the inactivation process, we performed a linear energy analysis of all the point mutations we have constructed in this study (Fig. 10). For these plots, energetic changes in N-terminal mutants were compared with the energetics of the appropriate base construct: wild type, V135K, V135D, EDE(161–3)AAA, or EDE(161–3)KKK. Fig. 10 shows that almost all the mutations in the polar region cluster tightly along the $\Phi = 0.91$, regardless of the base construct that the mutation was inserted into. A slope near 1 suggests that the entire polar region is consolidating at the same time during the main rate-liming step for inactivation. The only significant exception to this pattern occurs with residue 19, particularly the wild-type channel with the D19K substitution, which has a significant shift off of the $\Phi = 0.91$ line. This result could indicate that residue 19 plays a role later in the inactivation process, possibly affecting the manner in which the pore block reaction proceeds after polar region binding occurs.

Polar region binding and channel activation gating

Our studies support a model of polar region binding to the surface of the channel occurring early in the inactivation process and reversing late, after the rate-limiting step for recovery. A key question then is whether polar region binding is in constant equilibrium regardless of channel-gating state, or whether there is a binding cycle within the channel linked to channel activation gating. One possible way to distinguish between these options would be to determine if polar region mutations alter channel activation gating. If the charge at residue 18 regulates activation gating, this would be a strong indicator that the polar region must be prebound to the channel core before activation. To perform this test, we took advantage of an unexpected side effect of mutations to EDE(161–3), where charge-changing mutations of these residues produce a strong shift in activation gating (Fig. 11 A). If we compare the magnitude of the shift to the charge of the residues at 161–3, we see a clear electrostatic effect, where the activation curve shifts by around −9 mV as the residues at 161–3 are

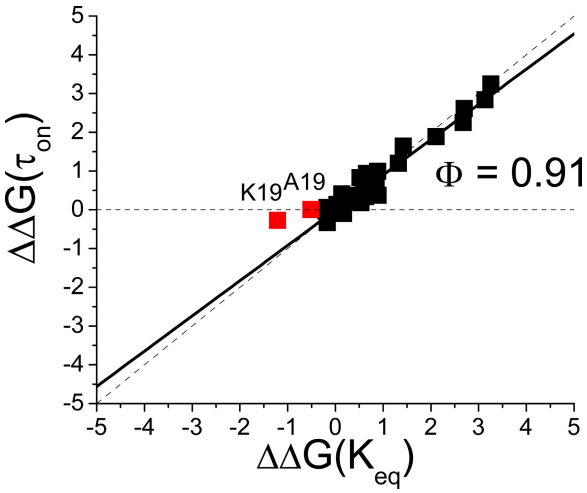

Figure 10. Linear energy plot for all mutations made to polar region–charged residues. In Tables II and IV, values for energetic effects of polar region mutations on τ_{on} and K_{eq} are plotted. Plot shows the change in on and equilibrium energy compared with the base construct for every mutation we constructed in the polar region of the AKv1 N terminus. Mutations cluster tightly near the Φ =1 line with a slope of 0.91, indicating that as a group, polar region mutations primarily impact a step early in the inactivation process and do not alter the energetics for recovery. Residue 19 mutations may be plotting along a shallower line, indicating that they also affect a later step in the inactivation process.

made progressively more positive (Fig. 11 B). This shift occurs without any apparent change in activation slope and therefore appears to be equivalent to a "surface charge" effect, where more positive residues at 161–3 convince the channel voltage sensor that the internal potential is more positive than it really is.

Because residue 18 has strong electrostatic coupling to 161–3, we reasoned that if residue 18 is bound to 161–3 in the closed state, the charge on residue 18 might alter the shift produced by EDE(161–3)KKK. We therefore tested whether changing the charge of residue 18 alters the shift in the activation curve produced by EDE(161–3)KKK. The results show that the charge at residue 18 has no discernable effect on the channel activation curve (Fig. 11 C). The shift in activation midpoint produced by EDE(161–3)KKK is not altered at all by the charge on residue 18 (Fig. 11 D), suggesting that the voltage sensor is not affected by the charge at position 18, and thus interactions between residue 18 and 161–3 are likely rare before channel activation gating.

Latch region mutant tail currents

The mutant EVA(2–4)ATT produces a rapid, partial inactivation with a large, sustained non-inactivating current (Fig. 3 D). An important open question, however, is the state of the N terminus in the sustained current channel population: Are these non-inactivated channels with an unbound N terminus, or is the bound N terminus inefficient in producing pore block? If the N terminus is largely unbound in these conducting channels, the tail currents should have two exponential components: a large, fast kinetic matching the normal closing of channels that are not inactivated, and a small, slower kinetic reflecting the fraction of channels that are N-type inactivated and recover through the open state. In this case, the peak conductance of the fast kinetic component should match the conductance for the sustained current component, and the closing

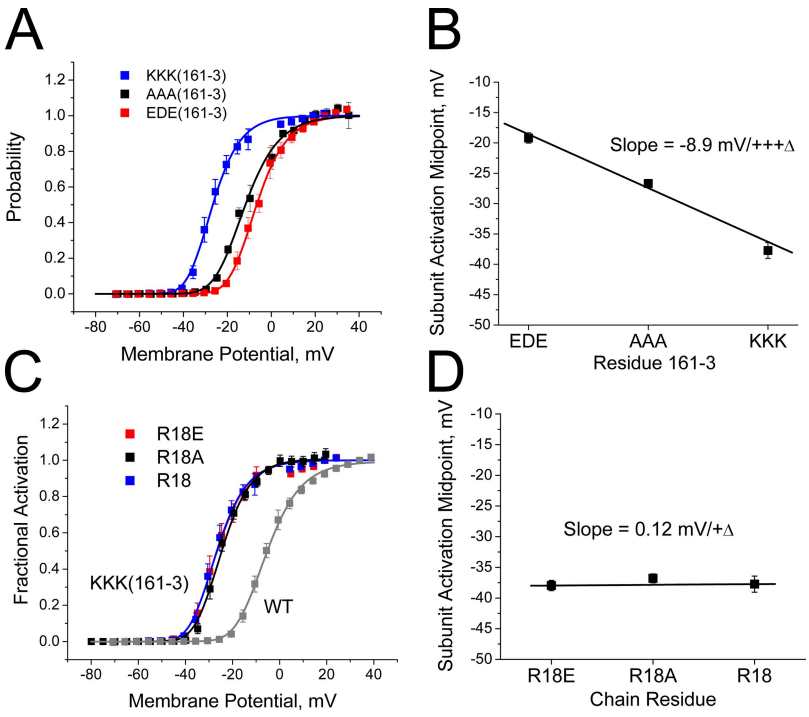

Figure 11. Charge at residue 161–3, but not at residue 18, affects voltage dependence for activation. (A) Activation curves for channels with different charges at residues 161–3 show a strong shift in activation with changes in charge at this site. Activation curves fit with fourth-power Boltzmann functions. (B) Plot of midpoint for subunit activation taken from fourth-power Boltzmann fits to the activation data for different charge substitutions at residue 161–3. Linear plot shows a clear electrostatic effect with an ~−9-mV shift in activation for neutral to positive change at these residues. (C) Effect of changing residue 18 charge on inactivation produced by 161–3 (KKK). Results show that the activation curves with different residue 18 charges stack on top of one another. (D) Plot of midpoint for subunit activation shows no effect of residue 18 charge on channel activation.

kinetics should match those of the AKv1(Δ2-57) channel that lacks an N-type inactivation domain. The magnitude of the slower component should be no larger than the total conductance for the fraction of channels that are inactivated, and the kinetics should match the kinetics for recovery from inactivation.

We therefore examined the tail currents from EVA(2–4)ATT channels during recovery from inactivation at −100 mV. As can be seen in Fig. 12 A, EVA(2–4)ATT channels produce large single-exponential tail currents; however, the decay kinetics for these tail currents are much slower than those seen for the closing of AKv1(Δ2-57) channels (Fig. 12 B). The decay time constant for the EVA(2–4)ATT tails closely matches the recovery time constant for EVA(2–4)ATT (see Table I), suggesting that these tails are produced by inactivated channels. Surprisingly, the peak conductance for the tail currents is more than two times bigger than the estimated conductance for the fraction of channel that inactivated during the depolarization and in fact matches the conductance for the sustained current component (Fig. 12 C). It therefore appears that the sustained channel component is not a separate population of channels with free N termini. Rather, all channels close in the same manner, as if they are all polar region bound and in an inactivated state that is beyond the rate-limiting step to recover, but only partially pore blocked.

DISCUSSION

Previous models for N-type inactivation have divided the N terminus up into an active region comprising approximately the first 20 residues of the N terminus and a chain region (Hoshi et al., 1990; Zhou et al., 2001). The chain region was presumed to be flexible but otherwise inert in the actual inactivation process. Even in the preinactivation model of the Kvβ1.1 N terminus, the N-terminal preinactivation site was seen to be distinct from the chain. Our results suggest that these functional divisions are likely incorrect and, furthermore, that the entire chain region plays a more active role in N-type inactivation.

Sequence analysis identifies three homology blocks within N-type inactivating Kv1 channels conserved from Drosophila and Aplysia to tunicate and vertebrates: latch, flex, and polar regions. Sequence similarity within the latch and flex regions is high enough to determine a 12-residue consensus sequence that is dominated by hydrophobic residues in the latch region and glycine residues in the flex region. The polar region, although showing less specific sequence homology, does display a charge conservation pattern that is evident in an acidic to basic shift in charged residues toward the N terminus of the polar region.

Based on these conserved sequence differences, we hypothesized that the latch, flex, and polar regions play distinct functional roles during N-type inactivation. Linear energy analysis suggests that the latch and flex region mutations can both modulate how the rate-limiting transition event occurs and have a major impact late in the inactivation reaction after the rate-limiting step. This suggests that these two regions of the N terminus may act together as a single functional unit to block the pore. In contrast, polar region mutations clearly affect an earlier phase in the inactivation process, suggesting that they have a distinct functional role that is largely completed by the time the rate-limiting step for inactivation is overcome.

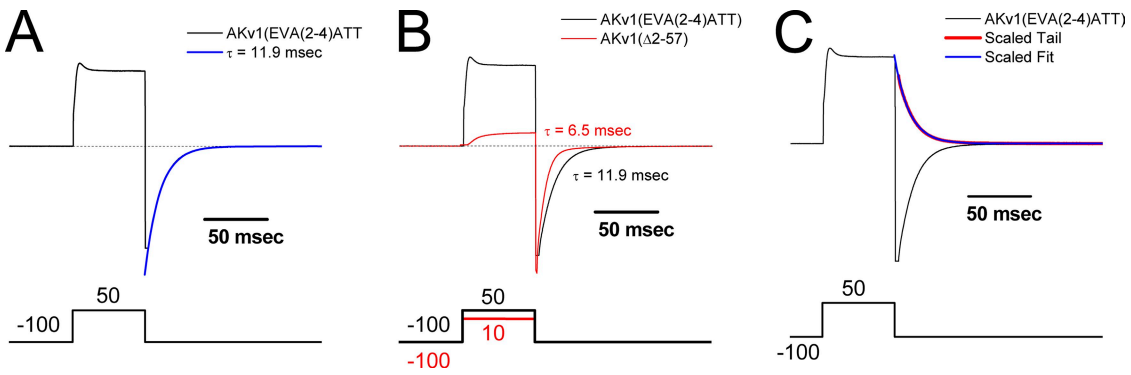

Figure 12. Tail currents for EVA(2–4)ATT mutant show all N termini have progressed beyond the inactivation rate-limiting step. Currents and voltage commands for tail current recordings for AKv1(EVA(2–4)ATT) and AKv1(Δ2-57) mutants. Pulse potentials given in mV. Zero current potentials are −5 mV. (A) EVA(2–4)ATT mutant has surprisingly large tail currents given the relatively small amount of current decay. Entire tail current is well fit with a single-exponential function with a tau closely matching the time constant for recovery from inactivation. (B) Tail currents for AKv1(EVA(2–4)ATT) and AKv1(Δ2-57) are aligned and scaled. In the absence of an N-terminal inactivation domain, AKv1(Δ2-57) channel tails decay twice as fast as AKv1(EVA(2–4)ATT) tails. (C) AKv1(EVA(2–4)ATT) tail currents are driving force normalized to plot versus the amplitude of the current at +50 mV. Single-exponential component tails are similar in size to the sustained component at +50 mV.

Polar region as a "sticky" chain

Extensive electrostatic interactions are found to occur throughout the polar region with the channel surface. Although the impact of mutations in the 16–25 region of the N terminus are typically larger than those to residues further from the N terminus, they do not act substantively differently from other polar region mutations, which all consolidate into the final inactivated structure at the same time as the 16–25 region, early in the inactivation process. Although our observations could be specific to the AKv1 channel, they are in substantial agreement with deletion studies performed on the chain region of the rKv1.4 channel (Wissmann et al., 2003). Given the close homology between the AKv1 N terminus and other N-type N termini, including Kv1.4 channels, it seems likely that binding interactions between the polar region and the channel core are an important conserved function.

The binding interaction between the polar region and the channel core appears to involve both electrostatic and non-electrostatic interactions. Based on the magnitude of the effects of our poly-Ala scanning mutations and our specific mutations to charged polar region residues, we estimate that the polar region contributes ∼6.5 kT of binding energy to the inactivation process, of which ∼4 kT is contributed by electrostatic interactions of charged residues with the channel surface (Fig. 13). The entire polar region interacts with a substantial electrostatic gradient that is directed in a positive to negative orientation toward the pore block site (Fig. 7 G). A switch from predominately acidic residues in the C terminus of the polar region to basic residues toward the N terminus of the polar region complements this electrostatic gradient and provides a substantial orienting effect that should act similarly to the diffuse steering potential predicted in experiments using inactivation ball peptides; however, in our studies, the electrostatic interactions with the N terminus are very residue specific, suggesting a specific binding site on the channel surface (Murrell-Lagnado and Aldrich, 1993a). This difference is not surprising given that a native inactivation domain is tethered at the C terminus, with extensive polar interactions that were not included in inactivation ball peptides; therefore, it binds in a more constrained manner.

The remaining non-electrostatic interactions are primarily formed by residues in the 16–25 region of the N terminus, contributing ∼2.3 kT of interaction energy. The largest electrostatic interaction we identified is felt by the most N-terminal polar region positive charge, R18, which experiences a potential change of greater than −30 mV upon reaching its binding site. At least half of this electrostatic potential appears to come from the negatively charged sequence EDE(161–3), which makes its strongest interaction with R18. This interaction occurs in a similar manner to a preinactivation interaction described for Kvβ1.1 (Zhou et al., 2001), strongly suggesting that the polar domain binding reaction we are describing here is functionally homologous to the preinactivation reaction described for Kvβ1.1.

The preinactivation site model proposed that the rate-limiting step for inactivation is determined by the time required for the N terminus to bind to the preinactivation site (Zhou et al., 2001). This would suggest that polar region binding is the rate-limiting step for N-type inactivation; however, estimates for the time to first collision between the N terminus and a target the size of the pore mouth suggest that a randomly diffusing N terminus attached to a chain should collide with the pore in <1 msec (Borys and Grzywna, 2008). Indeed, the ShB channel inactivation time constant is around this fast (Hoshi et al., 1990). It therefore does not seem likely that polar region binding to the channel surface is the rate-limiting step for the inactivation on reaction, which should likewise occur with sub-millisecond kinetics. Rather, it seems most likely that the rate-limiting step occurs after polar region binding and is dependent on the equilibrium constant for the binding reaction

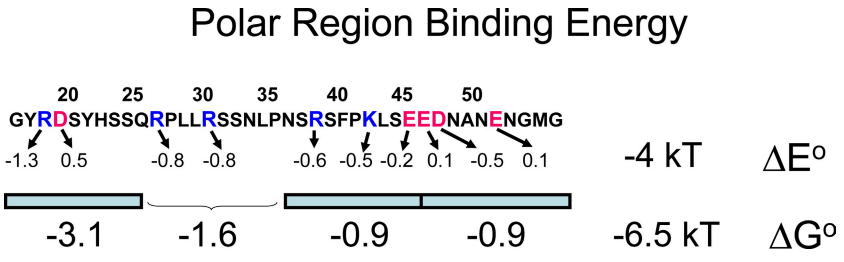

Figure 13. Summary of the polar region binding energetics. Sequence of AKv1 N-terminal polar region shown with charged residues highlighted. Arrows point toward the estimated equilibrium binding energy provided by the charged residue, in kT. Total estimated electrostatic equilibrium binding energy for all charged residues, ΔE^o, is around −4 kT. Poly-Ala scanning regions are shown by blue bars, with estimated binding energies for the probed regions provided below the bar, in kT. For the 26–45 region, binding energy is estimated from the charged residue contributions. The total binding energy contributed by the polar region, ΔG^o, is ∼−6.5 kT. Most of the missing −2.5 kT comes from non-electrostatic interactions occurring in the 16–25 region.

rather than the forward reaction rate. We hypothesize that the critical rate-limiting step involves movement of the latch region into the side window openings past a region of large negative charge (around −30 mV) identified by residue 18 binding energetics. This hypothesis provides a likely explanation for why our EVA(2–4)ATT mutation has a catalytic effect on the inactivation time course, whereas previous Kvβ1.1 mutations in this region did not. The EVA(2–4)ATT mutation removes a negative charge from the latch region, thus lowering the transition energy at the negatively charged side windows openings, whereas previous Kvβ1.1 mutations in this region did not affect the charge in the latch region (Zhou et al., 2001).

Functional significance of polar region binding

NMR studies suggest that the AKv1 N terminus interacts with the surface of the T1 domain, but that the interaction is of low affinity (Baker et al., 2006). The functional impact of the polar region interaction energy is predicted to be large, however, compared with the condition that would occur if there was no polar region binding interaction (I_0 condition). If we consider the simple conformational reaction between two states, free (F) and bound (B), that are randomly occupied based on a Markov process with associated probabilities P_B and P_F, then without any further information about this process, we can define an equilibrium constant for this reaction as:

$$K_{eq}(I_0) = \frac{P_B}{P_F} = \exp\left(\frac{-X^o kT}{kT}\right),$$

where X^o is the standard free energy between these states solely based on the probability to be in state B versus state F. Because energies add, the equilibrium constant for this same reaction, with the added condition that the inactivation domain has a polar region binding affinity of −6.5 kT for the B state (I_{PB} condition), is:

$$K_{eq}(I_{P_B}) = \frac{P_B}{P_F} = \exp\left(\frac{-(-6.5 + X^o)kT}{kT}\right).$$

If we take the ratio of these two equilibrium constants, we get:

$$\frac{K_B(I_{P_B})}{K_B(I_0)} = \exp\left(\frac{-(-6.5 + X^o)kT}{-X^o kT}\right) = \exp(6.5) > 650.$$

Thus, the stickiness of the polar region chain increases the equilibrium constant for preinactivation site binding by a factor of 650 over what the occupancy would be like if there were no polar region interactions. Given our wild-type time constant to inactivate of ∼30 msec, and a polar-binding equilibrium that favors the free state, this would suggest that without polar region interactions the time constant to inactivate for the AKv1 channel could be as long as 20 s.

The polar region binding site

Our ability to predict the entire set of channel core residues that are responsible for producing the electronegative potential gradient that is sensed by the N terminus is limited by our lack of knowledge of the C-terminal structure of Kv channels, which in AKv1 is composed of ∼20% charged residues (Pfaffinger et al., 1991). However, if we restrict our analysis to the T1 domain region of the channel, it is clear that the electrostatic potentials at the surface of this domain roughly produce a positive to negative potential track heading toward the transmembrane pore (Fig. 14 A). Previous NMR studies suggest that the N terminus of AKv1 remains mostly unstructured even in the presence of the T1 domain (Baker et al., 2006); however, the experienced potential change drops relatively slowly down the chain (e-fold per 16.6 residues) (Fig. 7 D). Given a Debye length of ∼9 Å, this suggests either a very compact polar region secondary structure in the bound state, such as an α helix, or multiple negative surface charges interacting along the polar region (Hille, 2001). The related Kv1.4 N terminus does form α-helical elements that are likely involved in interactions with the channel surface (Wissmann et al., 2003). If we assume that similar elements might form in the bound structure for the AKv1 polar region, we can thread the polar region of the AKv1 N terminus onto an α-helical template and ask how this structure maps onto the T1 domain surface (Fig. 14 B). Interestingly, this mapping places the positive charges along one side of the polar region, with D19 facing the opposite direction (Fig. 14 B). If we take this putative electrostatic footprint of the polar region and run it along the track in Fig. 14 A, we can see that when residue 18 is aligned with residues 161–3, there are good complementarities between the polar region footprint and the surface of the T1 domain (Fig. 14 C). Even residue D19, which translates into a region of largely negative potential during inactivation, appears to settle into a local positive maximum, which may help further refine the localization of the N terminus on the channel surface.

A unified framework for N-type inactivation

Tail current analysis of the EVA(2–4)ATT channel shows that the non-inactivated current seen with this mutant is not produced by channels that gate as if the N terminus is free. If this were the case, the tail currents would contain two components: one that matched the closing kinetic for channels lacking N-type inactivation, and the other matching channels that are recovering from N-type inactivation. Instead, we observe a single-exponential tail current closing kinetic that matches the time

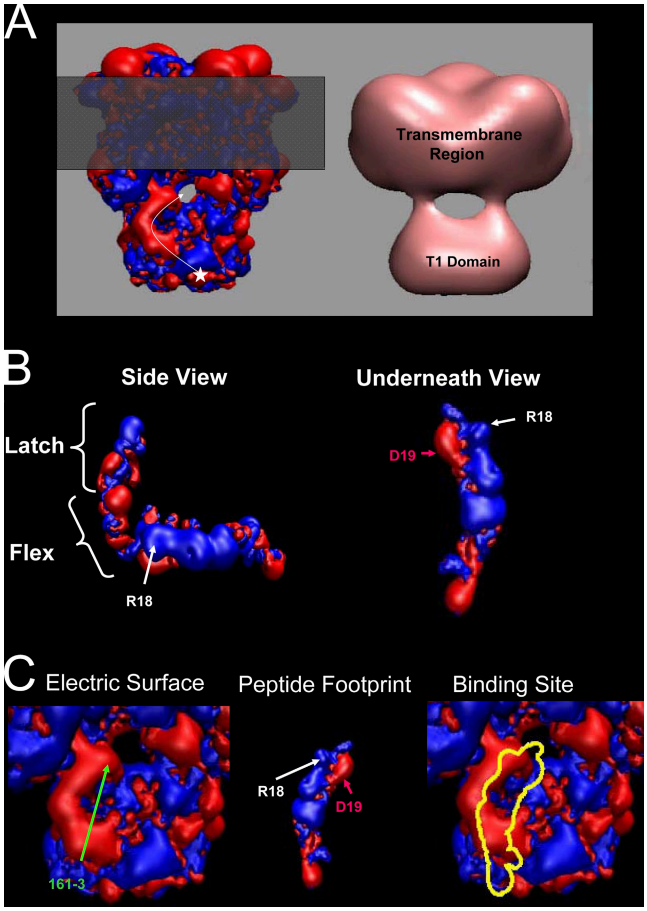

Figure 14. Structural models of the AKv1 channel identifying a potential polar region binding site on the channel surface. (A) Poisson-Boltzmann calculations of electric fields (isopotential surfaces: red, −1 kT/z; blue, +1 kT/z) emanating from the surface of the AKv1 protein (left) compared with an EM reconstruction of a Kv1 channel on the right (Sokolova et al., 2001) showing the side windows that provide access to the pore block site. The grayed-out region is assumed to be inaccessible to the N terminus due to the lipid bilayer. Star indicates the N-terminal end of the T1 domain where the N-type inactivation domain attaches to the channel. White arrow traces a possible path to the side window that shows a strong increase in negative potential as the arrow approaches the side window. (B) ±1-kT/z electrostatic surfaces for the AKv1 N terminus based on the Kv1.4 N terminus model (Wissmann et al., 2003). Flex and latch regions are not explicitly modeled due to flexibility in the Kv1.4 N-terminal model in this region. Bottom surface of the model (Underneath View) shows the presumed polar region interaction surface. The model shows how the polar region might expose a progression of positive charges to one side of an α-helical structure with D19 pointed in the opposite direction. (C) N terminus–T1 domain interaction model constructed by overlaying R18 and EDE(161–3) along the track proposed in A. Electric Surface: ±1-kT/z electrostatic surfaces for the channel Poisson-Boltzmann model focusing on the T1 domain. Peptide Footprint: Underneath N-terminal model in B is flipped horizontally to show how the exposed polar region electrostatic surface might interact with the T1 domain. Binding Site: Outline of the Peptide Footprint showing the T1 domain electrostatic potentials that underlie the proposed polar region binding site. Although the precise binding site is not known, this analysis indicates that a region of negative charge on the T1 domain surface complements the positively charged side of the polar region model. In addition, D19 points away from 161–3 toward a region of locally positive potential.

constant for recovery from inactivation. The observed tail currents produced by EVA(2–4)ATT are of such a large size that they could only be produced by also involving conductive channels that close as if they are recovering from the inactivated state. This result cannot be explained by a single-step inactivation model, but rather requires that the N terminus in the conductive population of EVA(2–4)ATT channel is in a state beyond the rate-limiting step, but not pore blocked. Therefore, at least two states must be available for the N terminus after the rate-limiting step is crossed: a conductive pre-block state and the actual pore block state. The single-exponential nature of the recovery from inactivation and large amplitude would occur if the pre-block and pore block states in this mutant are in rapid equilibrium relative to the rate-limiting step to recover, producing pseudo first-order reaction kinetics.

In Fig. 15, we show a simple inactivation gating cycle that is able to explain our observed results. After activation gating, the polar region rapidly binds to the surface of the channel, creating the open polar-bound ($O_{(P_B)}$) state. This state is in a rapid binding and unbinding equilibrium that limits how fast the next rate-limiting step can be overcome. Only if the open polar-bound ($O_{(P_B)}$) state is present can the rate-limiting transition occur that allows the latch and flex regions to work together to block the pore. The rate-limiting transition likely involves the latch region passing the negatively charged side window opening. After the rate-limiting step, our data suggest that there are two states in relatively rapid equilibrium: a pre-block and a pore block state. The pre-block state is still conductive and appears to be distinct from the previously proposed preinactivation site, which we have identified with the polar-bound state. Recovery appears to occur from the pre-block state because the EVA(2–4)ATT channels that are conductive recover identically to inactivated channels, and recovery kinetics increase as the fraction of pre-block channel present increases.

Based on our pre-block hypothesis and the need to form the polar region–bound state to transition to the pre-block state, it is likely that once the rate-limiting transition is crossed, the majority of the channels have a polar region in the bound state. It is currently unclear whether channel closing can occur before the complete unbinding of the inactivation domain from the polar region binding site. Given our proposed rapid kinetics for polar region unbinding, based on the low affinity, this kinetic cannot be resolved in our experiments. Our analysis showing that activation is insensitive to charge present at polar region position 18 suggests that it is

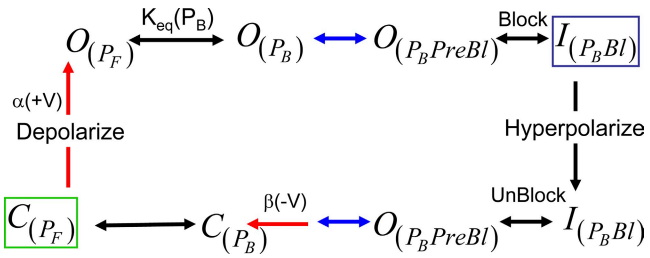

Figure 15. A multistate N-type inactivation model. Model shows gating cycle driven by depolarization and hyperpolarization. Blue, rate-controlling reactions; red, unidirectional reactions; black, reactions in rapid equilibrium. Stable state at depolarized potential is boxed in blue, and at hyperpolarized potentials is boxed in green. Depolarization triggers gating charge movement, which opens the channel (α(+V)) and exposes the polar region binding site. After polar region binding (P_B) to the open state, the channel is able to overcome the rate-limiting step to inactivate. Formation of the P_B intermediate is a key step in inactivation. At least two additional states exist after the rate limiting on transition is completed, a pre-block (*PreBl*) and a pore block (*Bl*) state. Both pre-block and pore block recover as if they are inactivated, but only the pore block state fails to conduct. For the recovery reaction, after membrane hyperpolarization, the pre-block and pore block states likely recover by a rate-limiting transition from the pre-block state. The exact order of steps to recover from pre-block are not clear, but it is likely that polar region unbinding occurs very rapidly once the channel closes (β(−V)) due to the low affinity binding.

unlikely that a significant fraction of the channels bind polar regions in the closed state.

The precise role of the flex region in N-type inactivation remains to be elucidated. Several recent papers have suggested that a β turn in the flex region might be required for proper formation of the inactivated, pore-blocked structure (Fernandez-Ballester et al., 1995; Decher et al., 2008; Molina et al., 2008). If so, our secondary structural analysis suggests that the AKv1 N terminus is certainly capable of adopting a flex region β turn, as are the other inactivation domains in Fig. 2 B. Glycine residues in the flex region may also be important for recovery because Kvβ1.1, which lacks glycine residues in the flex region, and our (7–15)Ala mutation, which removes flex region glycines, both recover from inactivation much more slowly than channels that contain flex region glycines.

In conclusion, our studies demonstrate that N-type inactivation involves the formation of a series of intermediate states that are differentially regulated by distinct regions of the N terminus. The majority of the N terminus is found to bind to a site on the surface of the channel leading up to the side window entrances to the pore. After this polar region binding, a rate-limiting conformation change puts the latch region in position to block the pore. These progressive interactions provide a likely explanation for how efficient inactivation of Kv1 channels occurs despite the apparently tortuous pathway that the N terminus must follow to reach the pore block binding site.

We thank Brian Nadin and Dr. Henry Jerng for their frequent scientific input and critical reading of this manuscript.

This research was supported by the National Science Foundation through TeraGrid resources provided by TACC Lonestar, and by National Institutes of Health grants R01NS31583 and P01NS37444.

Angus C. Nairn served as editor.

Submitted: 20 February 2009
Accepted: 20 May 2009

REFERENCES

Aldrich, R.W. 2001. Fifty years of inactivation. *Nature.* 411:643–644.

Antz, C., M. Geyer, B. Fakler, M.K. Schott, H.R. Guy, R. Frank, J.P. Ruppersberg, and H.R. Kalbitzer. 1997. NMR structure of inactivation gates from mammalian voltage-dependent potassium channels. *Nature.* 385:272–275.

Baker, K.A., C. Hilty, W. Peti, A. Prince, P.J. Pfaffinger, G. Wider, K. Wuthrich, and S. Choe. 2006. NMR-derived dynamic aspects of N-type inactivation of a Kv channel suggest a transient interaction with the T1 domain. *Biochemistry.* 45:1663–1672.

Baukrowitz, T., and G. Yellen. 1995. Modulation of K+ current by frequency and external [K+]: a tale of two inactivation mechanisms. *Neuron.* 15:951–960.

Borys, P., and Z.J. Grzywna. 2008. A diffusive model of the ball and chain inactivation. *Biosystems.* 94:267–269.

Choi, K.L., R.W. Aldrich, and G. Yellen. 1991. Tetraethylammonium blockade distinguishes two inactivation mechanisms in voltage-activated K+ channels. *Proc. Natl. Acad. Sci. USA.* 88:5092–5095.

Croarkin, C. 2008. NIST/SEMATECH e-Handbook of Statistical Methods. NIST.

Cushman, S.J., M.H. Nanao, A.W. Jahng, D. DeRubeis, S. Choe, and P.J. Pfaffinger. 2000. Voltage dependent activation of potassium channels is coupled to T1 domain structure. *Nat. Struct. Biol.* 7:403–407.

Decher, N., T. Gonzalez, A.K. Streit, F.B. Sachse, V. Renigunta, M. Soom, S.H. Heinemann, J. Daut, and M.C. Sanguinetti. 2008. Structural determinants of Kvbeta1.3-induced channel inactivation: a hairpin modulated by PIP2. *EMBO J.* 27:3164–3174.

Demo, S.D., and G. Yellen. 1991. The inactivation gate of the Shaker K+ channel behaves like an open-channel blocker. *Neuron.* 7:743–753.

Fernandez-Ballester, G., F. Gavilanes, J.P. Albar, M. Criado, J.A. Ferragut, and J.M. Gonzalez-Ros. 1995. Adoption of beta structure by the inactivating "ball" peptide of the Shaker B potassium channel. *Biophys. J.* 68:858–865.

Fersht, A.R., A. Matouschek, and L. Serrano. 1992. The folding of an enzyme. I. Theory of protein engineering analysis of stability and pathway of protein folding. *J. Mol. Biol.* 224:771–782.

Fuchs, P.F., and A.J. Alix. 2005. High accuracy prediction of beta-turns and their types using propensities and multiple alignments. *Proteins.* 59:828–839.

Furukawa, Y., and T. Takahashi. 1997. Comparison of accumulative inactivation between the Aplysia K+ channel (AKv1.1a) and its amino-terminal deletion mutant. *Zoolog. Sci.* 14:397–408.

Giese, K.P., M. Peters, and J. Vernon. 2001. Modulation of excitability as a learning and memory mechanism: a molecular genetic perspective. *Physiol. Behav.* 73:803–810.

Gilboa, G., R. Chen, and N. Brenner. 2005. History-dependent multiple-time-scale dynamics in a single-neuron model. *J. Neurosci.* 25:6479–6489.

Guex, N., and M.C. Peitsch. 1997. SWISS-MODEL and the Swiss-PdbViewer: an environment for comparative protein modeling. *Electrophoresis.* 18:2714–2723.

Gulbis, J.M., M. Zhou, S. Mann, and R. MacKinnon. 2000. Structure of the cytoplasmic beta subunit-T1 assembly of voltage-dependent K+ channels. *Science.* 289:123–127.

Hille, B. 2001. Ion Channels of Excitable Membranes. Third edition. Sinauer Associates Inc., Sunderland, MA. 814 pp.

Hoshi, T., W.N. Zagotta, and R.W. Aldrich. 1990. Biophysical and molecular mechanisms of Shaker potassium channel inactivation. *Science.* 250:533–538.

Humphrey, W., A. Dalke, and K. Schulten. 1996. VMD: visual molecular dynamics. *J. Mol. Graph.* 14:33–38, 27–28.

Jerng, H.H., Y. Qian, and P.J. Pfaffinger. 2004. Modulation of Kv4.2 channel expression and gating by dipeptidyl peptidase 10 (DPP10). *Biophys. J.* 87:2380–2396.

Jerng, H.H., K. Kunjilwar, and P.J. Pfaffinger. 2005. Multiprotein assembly of Kv4.2, KChIP3 and DPP10 produces ternary channel complexes with ISA-like properties. *J. Physiol.* 568:767–788.

Jerng, H.H., A.D. Lauver, and P.J. Pfaffinger. 2007. DPP10 splice variants are localized in distinct neuronal populations and act to differentially regulate the inactivation properties of Kv4-based ion channels. *Mol. Cell. Neurosci.* 35:604–624.

Kurata, H.T., and D. Fedida. 2006. A structural interpretation of voltage-gated potassium channel inactivation. *Prog. Biophys. Mol. Biol.* 92:185–208.

Lee, T.E., L.H. Philipson, and D.J. Nelson. 1996. N-type inactivation in the mammalian Shaker K+ channel Kv1.4. *J. Membr. Biol.* 151:225–235.

Long, S.B., E.B. Campbell, and R. Mackinnon. 2005. Crystal structure of a mammalian voltage-dependent Shaker family K+ channel. *Science.* 309:897–903.

Long, S.B., X. Tao, E.B. Campbell, and R. MacKinnon. 2007. Atomic structure of a voltage-dependent K+ channel in a lipid membrane-like environment. *Nature.* 450:376–382.

Molina, M.L., F.N. Barrera, J.A. Encinar, M.L. Renart, A.M. Fernandez, J.A. Poveda, J. Santoro, M. Bruix, F. Gavilanes, G. Fernandez-Ballester, et al. 2008. N-type inactivation of the potassium channel KcsA by the Shaker B "ball" peptide: mapping the inactivating peptide-binding epitope. *J. Biol. Chem.* 283:18076–18085.

Murrell-Lagnado, R.D., and R.W. Aldrich. 1993a. Energetics of Shaker K channels block by inactivation peptides. *J. Gen. Physiol.* 102:977–1003.

Murrell-Lagnado, R.D., and R.W. Aldrich. 1993b. Interactions of amino terminal domains of Shaker K channels with a pore blocking site studied with synthetic peptides. *J. Gen. Physiol.* 102:949–975.

Ono, F., Y. Katsuyama, K. Nakajo, and Y. Okamura. 1999. Subfamily-specific posttranscriptional mechanism underlies K(+) channel expression in a developing neuronal blastomere. *J. Neurosci.* 19:6874–6886.

Pfaffinger, P.J., Y. Furukawa, B. Zhao, D. Dugan, and E.R. Kandel. 1991. Cloning and expression of an Aplysia K+ channel and comparison with native Aplysia K+ currents. *J. Neurosci.* 11:918–927.

Phillips, J.C., R. Braun, W. Wang, J. Gumbart, E. Tajkhorshid, E. Villa, C. Chipot, R.D. Skeel, L. Kale, and K. Schulten. 2005. Scalable molecular dynamics with NAMD. *J. Comput. Chem.* 26:1781–1802.

Rettig, J., S.H. Heinemann, F. Wunder, C. Lorra, D.N. Parcej, J.O. Dolly, and O. Pongs. 1994. Inactivation properties of voltage-gated K+ channels altered by presence of a beta-subunit. *Nature.* 369:289–294.

Roberds, S.L., and M.M. Tamkun. 1991. Cloning and tissue-specific expression of five voltage-gated potassium channel cDNAs expressed in rat heart. *Proc. Natl. Acad. Sci. USA.* 88:1798–1802.

Sokolova, O., L. Kolmakova-Partensky, and N. Grigorieff. 2001. Three-dimensional structure of a voltage-gated potassium channel at 2.5 nm resolution. *Structure.* 9:215–220.

Wang, W., J.K. Takimoto, G.V. Louie, T.J. Baiga, J.P. Noel, K.F. Lee, P.A. Slesinger, and L. Wang. 2007. Genetically encoding unnatural amino acids for cellular and neuronal studies. *Nat. Neurosci.* 10:1063–1072.

Wissmann, R., W. Bildl, D. Oliver, M. Beyermann, H.R. Kalbitzer, D. Bentrop, and B. Fakler. 2003. Solution structure and function of the "tandem inactivation domain" of the neuronal A-type potassium channel Kv1.4. *J. Biol. Chem.* 278:16142–16150.

Zagotta, W.N., T. Hoshi, and R.W. Aldrich. 1990. Restoration of inactivation in mutants of Shaker potassium channels by a peptide derived from ShB. *Science.* 250:568–571.

Zhou, M., J.H. Morais-Cabral, S. Mann, and R. MacKinnon. 2001. Potassium channel receptor site for the inactivation gate and quaternary amine inhibitors. *Nature.* 411:657–661.

Zhou, Y., J.E. Pearson, and A. Auerbach. 2005. Phi-value analysis of a linear, sequential reaction mechanism: theory and application to ion channel gating. *Biophys. J.* 89:3680–3685.